

Calculation for Electric Dipole Moments of Lepton and Neutron in the N-B-LSSM via the Mass Insertion Approximation

Shuang Di^{1,2,3}, Wei-Hang Zhang^{1,2,3}, Rong-Zhi Sun^{1,2,3},

Xing-Xing Dong^{1,2,3,4*}, Guo-Zhu Ning^{1,2,3†}, Shu-Min Zhao^{1,2,3‡}

¹ *Department of Physics, Hebei University, Baoding 071002, China*

² *Hebei Key Laboratory of High-precision Computation and
Application of Quantum Field Theory, Baoding, 071002, China*

³ *Hebei Research Center of the Basic Discipline for
Computational Physics, Baoding, 071002, China and*

⁴ *Departamento de Fisica and CFTP,
Instituto Superior Técnico, Universidade de Lisboa,
Av.Rovisco Pais 1,1049-001 Lisboa, Portugal*

(Dated: March 17, 2026)

arXiv:2603.14774v1 [hep-ph] 16 Mar 2026

* dongxx@hbu.edu.cn

† ninggz@hbu.edu.cn

‡ zhaosm@hbu.edu.cn

Abstract

In the N-B-LSSM, we calculate the electric dipole moments (EDMs) of lepton and neutron at the one loop level via the Mass Insertion Approximation (MIA). In the Standard Model (SM), charge parity (CP) violation originates only from the single phase of the Cabibbo-Kobayashi-Maskawa (CKM) matrix, and the predicted EDMs of lepton and neutron are far below the current experimental upper limits. Thus, EDMs serve as sensitive probes for exploring CP-violating phases in new physics.

The N-B-LSSM extends the Minimal Supersymmetric Standard Model (MSSM) by introducing right-handed neutrino superfields and additional singlet Higgs superfields, which enriches the particle spectrum and the sources of CP violation. We derive the one loop analytical expressions for lepton and quark EDMs, and reveal their dependence on model parameters such as g_{YB} , $\theta_{\mu H}$, $\theta_{1'}$, $\theta_{BB'}$ and $\tan\beta$. Numerical analyses demonstrate that within a reasonable parameter space, the EDMs of leptons (electron, muon, tau) and the neutron can satisfy the current experimental limitations. This study provides a systematic theoretical tool and numerical reference for exploring CP violation and new physics under the N-B-LSSM.

PACS numbers:

Keywords: N-B-LSSM, CP violation, electric dipole moment (EDM), Mass Insertion Approximation (MIA).

I. INTRODUCTION

The SM of particle physics is highly successful. In the SM, the only source of CP violation comes from a single phase in the CKM matrix[1–5]. This source predicts extremely small EDMs for fermions. The predicted values are far below current experimental limitations. This promotes new physics beyond the SM (BSM). BSM models can add new CP-violating phases, and those phases can enhance the EDMs of the lepton and neutron[6].

In recent years, the improvements in experimental techniques have significantly enhanced constraints on the EDMs of leptons and neutron. The current limits on the EDMs of leptons and neutron are as follows[7–11]

$$\begin{aligned} |d_e| &< 4.1 \times 10^{-30} \text{ e.cm, CL} = 90\% \\ |d_\mu| &< 1.8 \times 10^{-19} \text{ e.cm, CL} = 95\% \\ |d_\tau| &< [-1.03, 0.23] \times 10^{-17} \text{ e.cm, CL} = 95\% \\ |d_n| &< 1.8 \times 10^{-26} \text{ e.cm, CL} = 90\% \end{aligned} \tag{1}$$

These strict experimental results set strong limits on the new CP-violation mechanisms in BSM models and also make it important to calculate the EDMs in the new models.

Supersymmetry (SUSY) is a well-known extension of the SM. SUSY naturally introduces new CP-violating phases. Examples include the phase θ_3 of the gluino mass term m_g , and the phase θ_{μ_H} of the Higgsino mass term μ_H . These phases can support electroweak baryogenesis (EWB)[12–17]. At the same time, they can strongly enhance lepton and neutron EDMs[18]. Therefore, achieving sufficient CP violation while suppressing EDM contributions remains a central issue in SUSY model building[19].

In this paper, MSSM extensions with a local $U(1)_{B-L}$ gauge symmetry offer a richer structure. In this work, the N-B-LSSM denotes the next-to-minimal supersymmetric model with a local $B-L$ gauge group, whose gauge group is $SU(3)_C \times SU(2)_L \times U(1)_Y \times U(1)_{B-L}$. This model introduces right-handed neutrino superfields and additional singlet Higgs superfields on the basis of the Minimal Supersymmetric Standard Model (MSSM). On the one hand, light neutrino masses can be explained by the seesaw mechanism[20]. On the other hand, the vacuum expectation value (VEV) of the singlet field can generate an effective μ term, thereby alleviating the μ problem at the model level[21]. Importantly, gauge kinetic mixing between the two $U(1)$ factors is a characteristic feature of this class of models[22].

It modifies the mixing structure and interactions of gauge bosons and neutral gauginos, and thus can have an impact on the main EDM contributions[23].

In the N-B-LSSM, new physics contributions to lepton and quark EDMs are mainly induced by supersymmetric loop diagrams. Lepton EDMs receive contributions from neutralino – slepton and chargino – sneutrino loops. Quark EDMs and CEDMs are dominated by gluino – squark loops as well as neutralino – squark loops[8, 18]. Extended degrees of freedom include additional neutralinos and singlet Higgs states. New CP-violating phases link to soft-breaking parameters and effective μ couplings parameters. These two components significantly modify the magnitude of EDMs[24]. This enables observable signals in future experiments, while being consistent with current bounds.

This paper aims to compute lepton EDMs and the neutron EDM (induced by quark EDM, CEDM and Weinberg operator contributions) in the N-B-LSSM using the MIA. The MIA provides an intuitive understanding of parameter dependence, which helps to identify the main sources affecting the EDM predictions. In particular, we focus on CP-violating phases such as θ_3 , and systematically analyze the impact of parameters including g_B , g_{YB} , and the additional soft mass terms $m_{BB'}$ and $m_{B'}$ on the EDMs. Through numerical scans, we show that there exists a viable parameter space in which the EDMs of lepton and neutron satisfy the current experimental upper bounds, thereby providing effective constraints on the model parameters.

The structure of this paper is as follows: In Section 2, we briefly review the N-B-LSSM. Section 3 details the calculation of EDMs for lepton and neutron using the mass insertion approach. In Section 4, we present numerical results and discuss their implications for the EDMs of lepton and neutron, along with the relevant physical explanations. Finally, conclusions are provided in Section 5.

II. THE $N - B - LSSM$

The N-B-LSSM is defined by the local gauge group[25]

$$SU(3)_C \times SU(2)_L \times U(1)_Y \times U(1)_{B-L}. \quad (2)$$

Compared with the MSSM, the model introduces additional chiral superfields, including three gauge-singlet Higgs superfields $\hat{\chi}_1$, $\hat{\chi}_2$, \hat{S} , together with the corresponding fermionic

partners (singlinos), and an additional $U(1)_{B-L}$ gaugino \widetilde{B}' . After symmetry breaking, the singlet field S develops a nonzero VEV. Consequently, the superpotential term $\lambda\hat{S}\hat{H}_u\hat{H}_d$ generates an effective μ parameter,

$$\mu_{\text{eff}} = \frac{\lambda v_S}{\sqrt{2}}, \quad (3)$$

which alleviates the μ -problem of the MSSM. Throughout this work we assume R -parity conservation, which is automatically preserved in the N-B-LSSM due to the gauged $B-L$ symmetry. With the singlet sector, the neutral CP-even scalar fields of H_u , H_d , χ_1 , χ_2 and S mix into a 5×5 mass squared matrix. The most significant impact for EDM is that the additional singlet/gauge sectors alter the neutralino (and Higgs) mass spectra and the associated couplings, thereby introducing new CP-sensitive contributions to the one loop EDM amplitudes.

The superpotential of the N-B-LSSM is

$$\begin{aligned} W = & -Y_d \hat{d} \hat{q} \hat{H}_d - Y_e \hat{e} \hat{l} \hat{H}_d - \lambda_2 \hat{S} \hat{\chi}_1 \hat{\chi}_2 + \lambda \hat{S} \hat{H}_u \hat{H}_d \\ & + \frac{\kappa}{3} \hat{S} \hat{S} \hat{S} + Y_u \hat{u} \hat{q} \hat{H}_u + Y_\chi \hat{\nu} \hat{\chi}_1 \hat{\nu} + Y_\nu \hat{\nu} \hat{l} \hat{H}_u. \end{aligned} \quad (4)$$

Here $Y_{u,d,e,\nu,\chi}$ denote Yukawa coupling matrices, while λ , λ_2 , and κ are dimensionless couplings. The fields $\hat{\chi}_1$, $\hat{\chi}_2$, and \hat{S} are singlet Higgs superfields. Note that a term of the form $Y'_\nu \hat{\nu} \hat{l} \hat{S}$ is forbidden by gauge invariance, since the sum of the corresponding $U(1)_Y$ charges of $\hat{\nu}$, \hat{l} , and \hat{S} is nonzero. In the following EDM analysis, the gaugino/soft terms may carry complex phases after field redefinitions, providing potential sources of CP violation.

The VEVs of the Higgs fields H_u , H_d , χ_1 , χ_2 , and S are denoted by v_u , v_d , v_η , $v_{\bar{\eta}}$, and v_S , respectively. Two angles are defined as $\tan \beta = v_u/v_d$ and $\tan \beta_\eta = v_{\bar{\eta}}/v_\eta$. The explicit expressions of the two Higgs doublets and three Higgs singlets around their VEVs are

$$\begin{aligned} H_d^0 &= \frac{1}{\sqrt{2}} \phi_d + \frac{1}{\sqrt{2}} v_d + i \frac{1}{\sqrt{2}} \sigma_d, \\ H_u^0 &= \frac{1}{\sqrt{2}} \phi_u + \frac{1}{\sqrt{2}} v_u + i \frac{1}{\sqrt{2}} \sigma_u, \\ \chi_1 &= \frac{1}{\sqrt{2}} \phi_1 + \frac{1}{\sqrt{2}} v_\eta + i \frac{1}{\sqrt{2}} \sigma_1, \\ \chi_2 &= \frac{1}{\sqrt{2}} \phi_2 + \frac{1}{\sqrt{2}} v_{\bar{\eta}} + i \frac{1}{\sqrt{2}} \sigma_2, \\ S &= \frac{1}{\sqrt{2}} \phi_S + \frac{1}{\sqrt{2}} v_S + i \frac{1}{\sqrt{2}} \sigma_S. \end{aligned} \quad (5)$$

In the EDM calculation, the above VEVs determine the neutralino/Higgs mixings and thus enter the couplings relevant for the one loop neutralino–slepton and chargino–sneutrino contributions.

The soft SUSY-breaking terms of the N-B-LSSM are

$$\begin{aligned}
\mathcal{L}_{soft} = & \mathcal{L}_{soft}^{MSSM} - \frac{T_\kappa}{3} S^3 + \epsilon_{ij} T_\lambda S H_d^i H_u^j + T_2 S \chi_1 \chi_2 \\
& - T_{\chi, ik} \chi_1 \tilde{\nu}_{R,i}^* \tilde{\nu}_{R,k}^* + \epsilon_{ij} T_\nu H_u^i \tilde{\nu}_{R,i}^* \tilde{e}_{L,j} - m_\eta^2 |\chi_1|^2 - m_\eta^2 |\chi_2|^2 \\
& - m_S^2 |S|^2 - m_{\nu, ij}^2 \tilde{\nu}_{R,i}^* \tilde{\nu}_{R,j} - \frac{1}{2} \left(2M_{BB'} \tilde{B} \lambda_{\tilde{B}'} + \delta_{ij} M_{BL} \lambda_{\tilde{B}'}^2 \right) + h.c. . \quad (6)
\end{aligned}$$

Here $\mathcal{L}_{soft}^{MSSM}$ denotes the soft-breaking terms of the MSSM, with T_κ , T_λ , T_2 , T_χ and T_ν being the trilinear soft-breaking parameters. In our EDM analysis, the dominant CP-violating phases stem from complex soft-breaking parameters, specifically the gaugino mass parameters M_1 , M_2 , the mixing mass $m_{BB'}$, and complex trilinear terms. These phases induce CP-odd couplings and chirality flips in loop amplitudes, and the relevant chirality-changing insertions are introduced within the framework of the MIA.

TABLE I: The superfields in N-B-LSSM.

Superfields	$U(1)_Y$	$SU(2)_L$	$SU(3)_C$	$U(1)_{B-L}$
\hat{q}	1/6	2	3	1/6
\hat{l}	-1/2	2	1	-1/2
\hat{H}_d	-1/2	2	1	0
\hat{H}_u	1/2	2	1	0
\hat{d}	1/3	1	$\bar{3}$	-1/6
\hat{u}	-2/3	1	$\bar{3}$	-1/6
\hat{e}	1	1	1	1/2
$\hat{\nu}$	0	1	1	1/2
$\hat{\chi}_1$	0	1	1	-1
$\hat{\chi}_2$	0	1	1	1
\hat{S}	0	1	1	0

The particle content and charge assignments are summarized in Table I. In the chiral superfield notation, $\hat{H}_u = (\hat{H}_u^+, \hat{H}_u^0)^T$ and $\hat{H}_d = (\hat{H}_d^0, \hat{H}_d^-)^T$ denote the MSSM-like Higgs doublet superfields. The superfields \hat{q} and \hat{l} represent the left-handed quark and lepton

doublets, while \hat{u} , \hat{d} , \hat{e} , and $\hat{\nu}$ correspond to the up-type quark, down-type quark, charged lepton, and neutrino singlet superfields, respectively.

The gauge groups $U(1)_Y$ and $U(1)_{B-L}$ generally exhibit gauge kinetic mixing, which can be induced through RGEs even if it is set to zero at M_{GUT} . A basis transformation can be performed by an orthogonal rotation matrix R ($R^T R = 1$)[23, 26–28]. The covariant derivative can be expressed as

$$D_\mu = \partial_\mu - i \left(Y, B - L \right) \begin{pmatrix} g_Y & g'_{YB} \\ g'_{BY} & g'_{B-L} \end{pmatrix} \begin{pmatrix} B_\mu^Y \\ B_\mu^{BL} \end{pmatrix}, \quad (7)$$

where Y and $B - L$ denote the hypercharge and the $B - L$ charge, respectively. One may choose a basis such that

$$\begin{pmatrix} g_Y & g'_{YB} \\ g'_{BY} & g'_{B-L} \end{pmatrix} R^T = \begin{pmatrix} g_1 & g_{YB} \\ 0 & g_B \end{pmatrix}, \quad (8)$$

and consequently the $U(1)$ gauge fields are redefined as

$$R \begin{pmatrix} B_\mu^Y \\ B_\mu^{BL} \end{pmatrix} = \begin{pmatrix} B_\mu^Y \\ B_\mu^{BL} \end{pmatrix}. \quad (9)$$

In the neutralino sector, the mass matrix in the basis $(\tilde{B}, \tilde{W}^0, \tilde{H}_d^0, \tilde{H}_u^0, \lambda_{\tilde{B}'}, \tilde{\chi}_1, \tilde{\chi}_2, \tilde{S})$ is given by

$$m_{\chi^0} = \begin{pmatrix} M_1 & 0 & -\frac{1}{2}g_1 v_d & \frac{1}{2}g_1 v_u & M_{BB'} & 0 & 0 & 0 \\ 0 & M_2 & \frac{1}{2}g_2 v_d & -\frac{1}{2}g_2 v_u & 0 & 0 & 0 & 0 \\ -\frac{1}{2}g_1 v_d & \frac{1}{2}g_2 v_d & 0 & -\frac{1}{\sqrt{2}}\lambda v_S & -\frac{1}{2}g_{YB} v_d & 0 & 0 & -\frac{1}{\sqrt{2}}\lambda v_u \\ \frac{1}{2}g_1 v_u & -\frac{1}{2}g_2 v_u & -\frac{1}{\sqrt{2}}\lambda v_S & 0 & \frac{1}{2}g_{YB} v_u & 0 & 0 & -\frac{1}{\sqrt{2}}\lambda v_d \\ M_{BB'} & 0 & -\frac{1}{2}g_{YB} v_d & \frac{1}{2}g_{YB} v_u & M_{BL} & -g_B v_\eta & g_B v_{\bar{\eta}} & 0 \\ 0 & 0 & 0 & 0 & -g_B v_\eta & 0 & -\frac{1}{\sqrt{2}}\lambda_2 v_S & -\frac{1}{\sqrt{2}}\lambda_2 v_{\bar{\eta}} \\ 0 & 0 & 0 & 0 & g_B v_{\bar{\eta}} & -\frac{1}{\sqrt{2}}\lambda_2 v_S & 0 & -\frac{1}{\sqrt{2}}\lambda_2 v_\eta \\ 0 & 0 & -\frac{1}{\sqrt{2}}\lambda v_u & -\frac{1}{\sqrt{2}}\lambda v_d & 0 & -\frac{1}{\sqrt{2}}\lambda_2 v_{\bar{\eta}} & -\frac{1}{\sqrt{2}}\lambda_2 v_\eta & \sqrt{2}\kappa v_S \end{pmatrix} \quad (10)$$

This matrix is diagonalized by a unitary matrix N ,

$$N^* m_{\chi^0} N^\dagger = m_{\chi^0}^{\text{diag}}. \quad (11)$$

III. ANALYTICAL FORMULA

A. The Lepton EDM

Using the on-shell condition for the external leptons, the lepton EDM can be obtained through the effective Lagrangian as follows[30–32]

$$\mathcal{L}_{EDM} = -\frac{i}{2}d_l\bar{l}\sigma^{\mu\nu}\gamma_5 l F_{\mu\nu}. \quad (12)$$

where $F_{\mu\nu}$ is the electromagnetic field strength tensor, and l denotes the lepton field. This effective Lagrangian explicitly violates CP symmetry and therefore cannot appear at tree level in the fundamental interactions. However, in a CP-violating electroweak theory, it can be generated at least at the one-loop level.

The Feynman amplitude corresponding to the process $l_j \rightarrow l_i + \gamma$ is dominated by a set of CP-violating dimension-6 operators, whose contributions are much larger than those of higher-dimensional operators, which are suppressed by a factor of $m_l^2/M_{\text{SUSY}}^2 \sim (10^{-7}, 10^{-8})$. After imposing the on-shell conditions for the external leptons, only the specific operator combinations $\mathcal{O}_{2,3,6}^{L,R}$ give direct contributions to the lepton EDM, with their magnitudes determined by the corresponding Wilson coefficients $C_{2,3,6}^{L,R}$. These operators are constructed from the covariant derivative $D_\mu = \partial_\mu + ieA_\mu$ and the chiral projection operators $P_{L,R} = (1 \mp \gamma_5)/2$. The specific forms of those dimension 6 operators are[29]

$$\begin{aligned} \mathcal{O}_1^{L,R} &= \frac{1}{(4\pi)^2}\bar{l}(i\mathcal{D})^3 P_{L,R}l, & \mathcal{O}_2^{L,R} &= \frac{eQ_f}{(4\pi)^2}\overline{(i\mathcal{D}_\mu l)}\gamma^\mu F \cdot \sigma P_{L,R}l, \\ \mathcal{O}_3^{L,R} &= \frac{eQ_f}{(4\pi)^2}\bar{l}F \cdot \sigma\gamma^\mu P_{L,R}(i\mathcal{D}_\mu l), & \mathcal{O}_4^{L,R} &= \frac{eQ_f}{(4\pi)^2}\bar{l}(\partial^\mu F_{\mu\nu})\gamma^\nu P_{L,R}l, \\ \mathcal{O}_5^{L,R} &= \frac{m_l}{(4\pi)^2}\bar{l}(i\mathcal{D})^2 P_{L,R}l, & \mathcal{O}_6^{L,R} &= \frac{eQ_f m_l}{(4\pi)^2}\bar{l}F \cdot \sigma P_{L,R}l. \end{aligned} \quad (13)$$

In the N-B-LSSM, the one-loop corrections to the lepton electric dipole moment primarily originate from loop diagrams involving sleptons and gauginos (such as the neutralino χ^0 and the chargino χ^\pm) with new physics parameters. Moreover, due to the introduction of right-handed neutrino superfields, the mass spectrum and mixing structure of the sneutrinos become more complicated and may provide additional sources of CP violation. The EDM contributions are generally not proportional to a single mass ratio but are instead constrained by mixing matrix elements. Their magnitudes are highly sensitive to new CP-violating phases and parameters such as $\tan\beta$ in the model. To clearly reveal this parameter

dependence, it is particularly convenient to employ the MIA[33], which expresses the EDM contributions analytically as functions of the model parameters, thereby highlighting the origin of CP violation. Fig.1 shows the Feynman diagrams for the lepton EDM induced based on MIA.

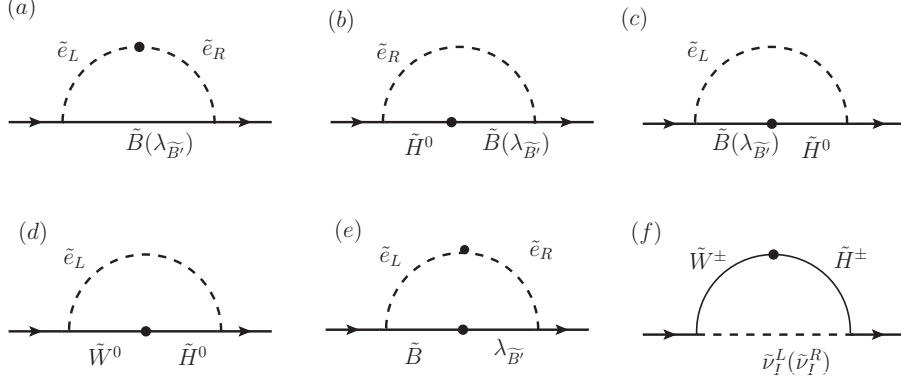


FIG. 1: Feynman diagrams for generating lepton EDM based on MIA. The external photons are connected to the charged internal lines in all possible ways.

In the following, within the N-B-LSSM and using the MIA, the explicit analytical forms of the one-loop contributions to the lepton EDM are presented here.

a. The one-loop contributions from \tilde{B} - \tilde{e}_L - \tilde{e}_R .

$$d_l^{(a)}(\tilde{e}_L, \tilde{e}_R, \tilde{B}) = \frac{eg_1^2}{M_{SUSY}} \sqrt{x_1 x_l x_{\mu H}} e^{i\theta_1} e^{i\theta_{\mu H}} \tan \beta I_1(x_1, x_{\tilde{e}_L}, x_{\tilde{e}_R}). \quad (14)$$

The one-loop contributions from $\lambda_{\tilde{B}}$ - \tilde{e}_L - \tilde{e}_R .

$$d_l^{(a)}(\tilde{e}_L, \tilde{e}_R, \lambda_{\tilde{B}}) = \frac{e(g_{YB} + g_B)(2g_{YB} + g_B)}{2M_{SUSY}} \sqrt{x_{\lambda_{\tilde{B}}} x_l x_{\mu H}} \times e^{i\theta_1} e^{i\theta_{\mu H}} \tan \beta I_1(x_{\lambda_{\tilde{B}}}, x_{\tilde{e}_L}, x_{\tilde{e}_R}). \quad (15)$$

The functions $I_1(x, y, z)$ are defined as

$$I_1(x, y, z) = \frac{1}{32\pi^2} \left\{ \frac{-3x^2 + yz + x(y+z)}{(x-y)^2(x-z)^2} + \frac{2x[x^3 - 3xyz + yz(y+z)] \log x}{(x-y)^3(x-z)^3} - \frac{2xy \log y}{(x-y)^3(y-z)} - \frac{2xz \log z}{(x-z)^3(z-y)} \right\}. \quad (16)$$

b. The one-loop contributions from \tilde{B} - \tilde{H}^0 - \tilde{e}_R .

$$d_l^{(b)}(\tilde{e}_R, \tilde{H}^0, \tilde{B}) = \frac{eg_1^2}{M_{SUSY}} \sqrt{x_1 x_l x_{\mu H}} e^{i\theta_1} e^{i\theta_{\mu H}} \tan \beta I_2(x_1, x_{\mu H}, x_{\tilde{e}_R}). \quad (17)$$

The one-loop contributions from $\lambda_{\tilde{B}'}-\tilde{H}^0-\tilde{e}_R$.

$$d_l^{(b)}(\tilde{e}_R, \tilde{H}^0, \lambda_{\tilde{B}'}) = \frac{eg_1(2g_{YB} + g_B)}{2M_{SUSY}} \sqrt{x_{\lambda_{\tilde{B}'}} x_l x_{\mu_H}} e^{i\theta'_1} e^{i\theta_{\mu_H}} \tan \beta I_2(x_{\lambda_{\tilde{B}'}} , x_{\mu_H}, x_{\tilde{e}_R}). \quad (18)$$

c. The one-loop contributions from $\tilde{B}-\tilde{H}^0-\tilde{e}_L$.

$$d_l^{(c)}(\tilde{e}_L, \tilde{H}^0, \tilde{B}) = -\frac{eg_1^2}{2M_{SUSY}} \sqrt{x_1 x_l x_{\mu_H}} e^{i\theta_1} e^{i\theta_{\mu_H}} \tan \beta I_2(x_1, x_{\mu_H}, x_{\tilde{e}_L}). \quad (19)$$

The one-loop contributions from $\lambda_{\tilde{B}'}-\tilde{H}^0-\tilde{e}_L$.

$$d_l^{(c)}(\tilde{e}_L, \tilde{H}^0, \lambda_{\tilde{B}'}) = -\frac{eg_1(g_{YB} + g_B)}{2M_{SUSY}} \sqrt{x_{\lambda_{\tilde{B}'}} x_l x_{\mu_H}} e^{i\theta'_1} e^{i\theta_{\mu_H}} \tan \beta I_2(x_{\lambda_{\tilde{B}'}} , x_{\mu_H}, x_{\tilde{e}_L}). \quad (20)$$

d. The one-loop contributions from $\tilde{W}^0-\tilde{H}^0-\tilde{e}_L$.

$$d_l^{(d)}(\tilde{e}_L, \tilde{H}^0, \tilde{W}^0) = \frac{eg_2^2}{2M_{SUSY}} \sqrt{x_2 x_l x_{\mu_H}} e^{i\theta_2} e^{i\theta_{\mu_H}} \tan \beta I_2(x_2, x_{\mu_H}, x_{\tilde{e}_L}). \quad (21)$$

The functions $I_2(x, y, z)$ is defined as

$$I_2(x, y, z) = \frac{1}{32\pi^2} \left\{ \frac{(y-3z)z + x(y+z)}{(x-z)^2(y-z)^2} + \frac{2xz \log x}{(x-y)(x-z)^3} \right. \\ \left. + \frac{2yz \log y}{(-x+y)(y-z)^3} - \frac{2z[xy(x+y) - 3xyz + z^3] \log z}{(x-z)^3(-y+z)^3} \right\}. \quad (22)$$

e. The one-loop contributions from $\lambda_{\tilde{B}'}-\tilde{B}-\tilde{e}_L-\tilde{e}_R$.

$$d_l^{(e)}(\tilde{e}_L, \tilde{e}_R, \lambda_{\tilde{B}'}, \tilde{B}) = -\frac{eg_1(g_{YB} + g_B)}{2M_{SUSY}} \sqrt{x_{BB'} x_{\mu_H}} e^{i\theta_{BB'}} e^{i\theta_{\mu_H}} \tan \beta \\ \times [\sqrt{x_1 x_{\lambda_{\tilde{B}'}}} f(x_{BB'}, x_1, x_{\tilde{e}_L}, x_{\tilde{e}_R}) - g(x_{BB'}, x_1, x_{\tilde{e}_L}, x_{\tilde{e}_R})]. \quad (23)$$

The functions $f(x, y, z, t)$ and $g(x, y, z, t)$ are defined as

$$f(x, y, z, t) = \frac{1}{16\pi^2} \left\{ \frac{t[t^3 + xy(x+y-3t)] \log t}{(t-x)^3(t-y)^3(t-z)} - \frac{x[x^3 + tz(t+z-3x)] \log x}{(t-x)^3(x-y)(x-z)^3} \right. \\ \left. + \frac{y[y^3 + tz(t+z-3y)] \log y}{(t-y)^3(x-y)(y-z)^3} - \frac{z[z^3 + xy(x+y-3z)] \log z}{(t-z)(z-x)^3(z-y)^3} \right. \\ \left. + \frac{1}{2(x-y)} \left[\frac{tx + tz + xz - 3x^2}{(t-x)^2(x-z)^2} - \frac{ty + tz + yz - 3y^2}{(t-y)^2(y-z)^2} \right] \right\}; \quad (24)$$

$$g(x, y, z, t) = \frac{1}{16\pi^2} \left\{ \frac{x(3x^2 - tx - tz - xz)}{2(t-x)^2(x-y)(x-z)^2} - \frac{y[t(y+z) + y(z-3y)]}{2(t-y)^2(y-x)(y-z)^2} \right. \\ \left. - \frac{t[t^3(x+y) - 3t^2xy + x^2y^2] \log t}{(t-x)^3(t-y)^3(t-z)} + \frac{z[x^2y^2 + xz^2(z-3y) + yz^3] \log z}{(t-z)(z-x)^3(z-y)^3} \right. \\ \left. + \frac{x^2[x^3 + tz(t+z-3x)] \log x}{(t-x)^3(x-y)(x-z)^3} - \frac{y^2[y^3 + tz(t+z-3y)] \log y}{(t-y)^3(x-y)(y-z)^3} \right\}. \quad (25)$$

f. The one-loop contributions from $\widetilde{W}^\pm\text{-}\widetilde{H}^\pm\text{-}\widetilde{\nu}_L^I$.

$$d_l^{(f)}(\widetilde{W}^\pm, \widetilde{H}^\pm, \widetilde{\nu}_L^I) = -\frac{eg_2^2}{2M_{SUSY}}\sqrt{x_2x_lx_{\mu_H}}e^{i\theta_2}e^{i\theta_{\mu_H}}\tan\beta I_3(x_2, x_{\mu_H}, x_{\nu_L^I}). \quad (26)$$

The one-loop contributions from $\widetilde{W}^\pm\text{-}\widetilde{H}^\pm\text{-}\widetilde{\nu}_L^R$.

$$d_l^{(f)}(\widetilde{W}^\pm, \widetilde{H}^\pm, \widetilde{\nu}_L^R) = -\frac{eg_2^2}{2M_{SUSY}}\sqrt{x_2x_lx_{\mu_H}}e^{i\theta_2}e^{i\theta_{\mu_H}}\tan\beta I_3(x_2, x_{\mu_H}, x_{\nu_L^R}). \quad (27)$$

The functions $I_3(x, y, z)$ are defined as

$$I_3(x, y, z) = \frac{1}{32\pi^2}\left\{\frac{xy(x^2+y^2)-3(x^3+y^3)z+6(x^2-xy+y^2)z^2-(x+y)z^3}{(x-y)^2(x-z)^2(y-z)^2}\right. \\ -\frac{x^3(x+y)-x^2(x+3y)z+2(x^2-xy+y^2)z^2\log x}{(x-y)^3(x-z)^3} \\ +\frac{y^3(x+y)-y^2(3x+y)z+2(x^2-xy+y^2)z^2\log y}{(x-y)^3(y-z)^3} \\ \left. +\frac{z^2(2x^2+xy+2y^2-5(x+y)z+5z^2)\log z}{(x-z)^3(-y+z)^3}\right\}. \quad (28)$$

The mass parameters of the superparticles ($M_1, M_2, \mu_H, m_{\widetilde{e}_L}, m_{\widetilde{e}_R}, m_{\widetilde{\nu}_L}, M'_1, M_3, m_{\widetilde{u}_L}, m_{\widetilde{u}_R}, m_{\widetilde{d}_L}, m_{\widetilde{d}_R}$) are assumed equal to M_{SUSY} to obtain the simple results,

$$|M_1| = |M_2| = |\mu_H| = m_{\widetilde{e}_L} = m_{\widetilde{e}_R} = m_{\widetilde{\nu}_L} = |M'_1| = |M_3| = m_{\widetilde{u}_L} = m_{\widetilde{u}_R} = m_{\widetilde{d}_L} = m_{\widetilde{d}_R} = M_{SUSY}. \quad (29)$$

The one-loop contributions to lepton EDM can be expressed as

$$d_l^e = d_l^{\widetilde{\chi}^0} + d_l^{\widetilde{\nu}\chi^\pm}, \\ d_l^{\widetilde{\chi}^0} \simeq d_l^{(a)}(\widetilde{e}_L, \widetilde{e}_R, \widetilde{B}) + d_l^{(a)}(\widetilde{e}_L, \widetilde{e}_R, \lambda_{\widetilde{B}'}) + d_l^{(b)}(\widetilde{e}_R, \widetilde{H}^0, \widetilde{B}) + d_l^{(b)}(\widetilde{e}_R, \widetilde{H}^0, \lambda_{\widetilde{B}'}) \\ + d_l^{(c)}(\widetilde{e}_L, \widetilde{H}^0, \widetilde{B}) + d_l^{(c)}(\widetilde{e}_L, \widetilde{H}^0, \lambda_{\widetilde{B}'}) + d_l^{(d)}(\widetilde{e}_L, \widetilde{H}^0, \widetilde{W}^0) + d_l^{(e)}(\widetilde{e}_L, \widetilde{e}_R, \lambda_{\widetilde{B}'}, \widetilde{B}), \\ d_l^{\widetilde{\nu}\chi^\pm} \simeq d_l^{(f)}(\widetilde{W}^\pm, \widetilde{H}^\pm, \widetilde{\nu}_L^I) + d_l^{(f)}(\widetilde{W}^\pm, \widetilde{H}^\pm, \widetilde{\nu}_L^R). \quad (30)$$

Some parameters are defined as follows

$$m_{\widetilde{B}} = M_1 * e^{i*\theta_1}, \quad m_{\widetilde{W}^0} = m_{\widetilde{W}^\pm} = M_2 * e^{i*\theta_2}, \quad \mu_H = \frac{\lambda v_S}{\sqrt{2}} = M_{\mu_H} * e^{i*\theta_{\mu_H}}, \\ m_{\lambda_{\widetilde{B}'}} = M'_1 * e^{i*\theta'_1}, \quad m_{BB'} = M_{BB'} * e^{i*\theta_{BB'}}, \quad x_i = \frac{|M_i|^2}{M_{SUSY}^2}. \quad (31)$$

$\theta_1, \theta_2, \theta_{\mu_H}, \theta_{1'},$ and $\theta_{BB'}$ are the CP-violating phases of the parameters $m_{\widetilde{B}}, m_{\widetilde{W}^0}$ ($m_{\widetilde{W}^\pm}$), $\mu_H, m_{\lambda_{\widetilde{B}'}}$ and $m_{BB'}$.

B. The Neutron EDM

The neutron EDM can also be obtained from the effective Lagrangian Eq.(12). The neutron is a composite particle composed of quarks and gluons. Its EDM arises not only from the quark EDM but also receives important contributions from the quark CEDM. This contribution is described by the operator $\bar{q}T^a\sigma_{\mu\nu}\gamma_5qG_a^{\mu\nu}$, where $G_a^{\mu\nu}$ is the gluon field strength tensor. In addition, Weinberg discovered a CP-violating dimension-6 gluonic operator $f_{abc}\tilde{G}_a^{\mu\nu}G_{b\mu}^\rho G_{c\rho\nu}$, which yields a large contribution to the neutron EDM.

The one loop diagrams for generating neutron EDM based on MIA are shown in Fig.2 and Fig.3.

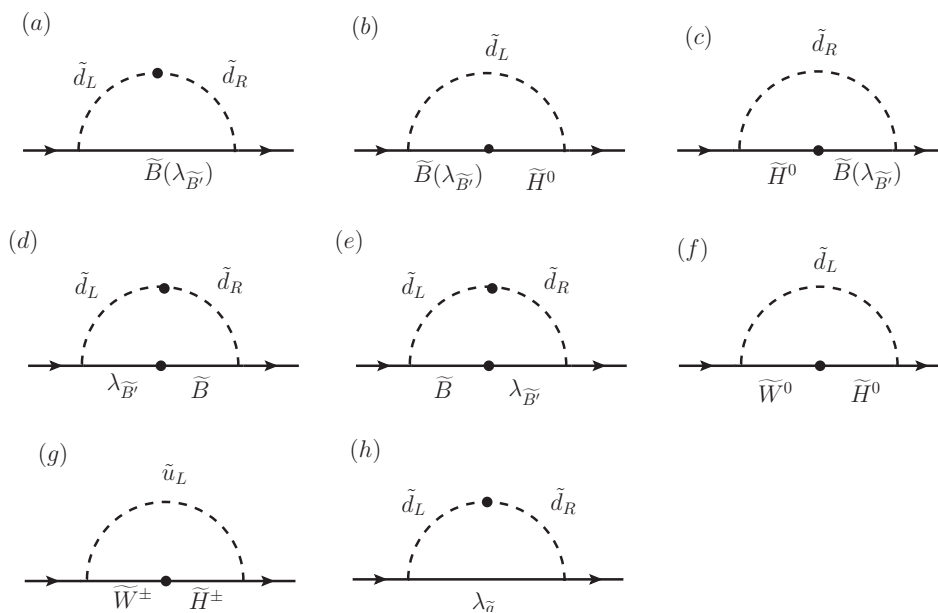


FIG. 2: Feynman diagrams of down-quark for generating neutron EDM based on MIA. External photons connect to charged internal lines in all possible ways, while external gluons connect to colored internal lines.

a. The one-loop contributions to the quark EDMs and CEDMs from $\tilde{B}-\tilde{d}_L-\tilde{d}_R$.

$$\begin{aligned}
 d_q^{(a)}(\tilde{d}_L, \tilde{d}_R, \tilde{B}) &= -\frac{eg_1^2}{27M_{SUSY}}\sqrt{x_1x_dx_{\mu H}}e^{i\theta_1}e^{i\theta_{\mu H}}\tan\beta I_1(x_1, x_{\tilde{d}_L}, x_{\tilde{d}_R}); \\
 d_q^{g(a)}(\tilde{d}_L, \tilde{d}_R, \tilde{B}) &= \frac{g_3g_1^2}{9M_{SUSY}}\sqrt{x_1x_dx_{\mu H}}e^{i\theta_1}e^{i\theta_{\mu H}}\tan\beta I_1(x_1, x_{\tilde{d}_L}, x_{\tilde{d}_R}).
 \end{aligned}
 \tag{32}$$

The one-loop contributions to the quark EDMs and CEDMs from $\lambda_{\tilde{B}'}-\tilde{d}_L-\tilde{d}_R$.

$$\begin{aligned}
d_q^{\gamma(a)}(\tilde{d}_L, \tilde{d}_R, \lambda_{\tilde{B}'}) &= \frac{e(g_{YB} + g_B)(-2g_{YB} + g_B)}{54M_{SUSY}} \sqrt{x_{\lambda_{\tilde{B}'}} x_d x_{\mu_H}} e^{i\theta_1} e^{i\theta_{\mu_H}} \tan \beta \\
&\quad I_1(x_{\lambda_{\tilde{B}'}} , x_{\tilde{d}_L} , x_{\tilde{d}_R}); \\
d_q^{g(a)}(\tilde{d}_L, \tilde{d}_R, \lambda_{\tilde{B}'}) &= -\frac{g_3(g_{YB} + g_B)(-2g_{YB} + g_B)}{18M_{SUSY}} \sqrt{x_{\lambda_{\tilde{B}'}} x_d x_{\mu_H}} e^{i\theta_1} e^{i\theta_{\mu_H}} \tan \beta \\
&\quad \times I_1(x_{\lambda_{\tilde{B}'}} , x_{\tilde{d}_L} , x_{\tilde{d}_R}).
\end{aligned} \tag{33}$$

b. The one-loop contributions to the quark EDMs and CEDMs from $\tilde{B}-\tilde{H}^0-\tilde{d}_L$.

$$\begin{aligned}
d_q^{\gamma(b)}(\tilde{d}_L, \tilde{H}^0, \tilde{B}) &= \frac{eg_1^2}{18M_{SUSY}} \sqrt{x_1 x_d x_{\mu_H}} e^{i\theta_1} e^{i\theta_{\mu_H}} \tan \beta I_2(x_1, x_{\mu_H}, x_{\tilde{d}_L}); \\
d_q^{g(b)}(\tilde{d}_L, \tilde{H}^0, \tilde{B}) &= -\frac{g_3 g_1^2}{6M_{SUSY}} \sqrt{x_1 x_d x_{\mu_H}} e^{i\theta_1} e^{i\theta_{\mu_H}} \tan \beta I_2(x_1, x_{\mu_H}, x_{\tilde{d}_L}).
\end{aligned} \tag{34}$$

The one-loop contributions to the quark EDMs and CEDMs from $\lambda_{\tilde{B}'}-\tilde{H}^0-\tilde{d}_L$.

$$\begin{aligned}
d_q^{\gamma(b)}(\tilde{d}_L, \tilde{H}^0, \lambda_{\tilde{B}'}) &= -\frac{eg_{YB}(g_{YB} + g_B)}{18M_{SUSY}} \sqrt{x_{\lambda_{\tilde{B}'}} x_d x_{\mu_H}} e^{i\theta_1} e^{i\theta_{\mu_H}} \tan \beta I_2(x_{\lambda_{\tilde{B}'}} , x_{\mu_H}, x_{\tilde{d}_L}); \\
d_q^{g(b)}(\tilde{d}_L, \tilde{H}^0, \lambda_{\tilde{B}'}) &= \frac{g_3 g_{YB}(g_{YB} + g_B)}{6M_{SUSY}} \sqrt{x_{\lambda_{\tilde{B}'}} x_d x_{\mu_H}} e^{i\theta_1} e^{i\theta_{\mu_H}} \tan \beta I_2(x_{\lambda_{\tilde{B}'}} , x_{\mu_H}, x_{\tilde{d}_L}).
\end{aligned} \tag{35}$$

c. The one-loop contributions to the quark EDMs and CEDMs from $\tilde{B}-\tilde{H}^0-\tilde{d}_R$.

$$\begin{aligned}
d_q^{\gamma(c)}(\tilde{d}_R, \tilde{H}^0, \tilde{B}) &= \frac{eg_1^2}{9M_{SUSY}} \sqrt{x_1 x_l x_{\mu_H}} e^{i\theta_1} e^{i\theta_{\mu_H}} \tan \beta I_2(x_1, x_{\mu_H}, x_{\tilde{d}_R}); \\
d_q^{g(c)}(\tilde{d}_R, \tilde{H}^0, \tilde{B}) &= -\frac{g_3 g_1^2}{3M_{SUSY}} \sqrt{x_1 x_l x_{\mu_H}} e^{i\theta_1} e^{i\theta_{\mu_H}} \tan \beta I_2(x_1, x_{\mu_H}, x_{\tilde{d}_R}).
\end{aligned} \tag{36}$$

The one-loop contributions to the quark EDMs and CEDMs from $\lambda_{\tilde{B}'}-\tilde{H}^0-\tilde{d}_R$.

$$\begin{aligned}
d_q^{\gamma(c)}(\tilde{d}_R, \tilde{H}^0, \lambda_{\tilde{B}'}) &= -\frac{eg_{YB}(-2g_{YB} + g_B)}{18M_{SUSY}} \sqrt{x_{\lambda_{\tilde{B}'}} x_l x_{\mu_H}} e^{i\theta_1} e^{i\theta_{\mu_H}} \tan \beta I_1(x_{\lambda_{\tilde{B}'}} , x_{\mu_H}, x_{\tilde{d}_R}); \\
d_q^{g(c)}(\tilde{d}_R, \tilde{H}^0, \lambda_{\tilde{B}'}) &= \frac{g_3 g_{YB}(-2g_{YB} + g_B)}{6M_{SUSY}} \sqrt{x_{\lambda_{\tilde{B}'}} x_l x_{\mu_H}} e^{i\theta_1} e^{i\theta_{\mu_H}} \tan \beta I_2(x_{\lambda_{\tilde{B}'}} , x_{\mu_H}, x_{\tilde{d}_R}).
\end{aligned} \tag{37}$$

d. The one-loop contributions to the quark EDMs and CEDMs from $\lambda_{\tilde{B}'}-\tilde{B}-\tilde{d}_L-\tilde{d}_R$.

$$\begin{aligned}
d_q^{\gamma(d)}(\tilde{d}_L, \tilde{d}_R, \lambda_{\tilde{B}'}, \tilde{B}) &= -\frac{eg_1(g_{YB} + g_B)}{18M_{SUSY}} \sqrt{x_d x_{BB'} x_{\mu_H}} e^{i\theta_{BB'}} e^{i\theta_{\mu_H}} \tan \beta \\
&\quad \times [\sqrt{x_1 x_{\lambda_{\tilde{B}'}}} f(x_{BB'}, x_1, x_{\tilde{d}_L}^0, x_{\tilde{d}_R}^0) - g(x_{BB'}, x_1, x_{\tilde{d}_L}, x_{\tilde{d}_R})]; \\
d_q^{g(d)}(\tilde{d}_L, \tilde{d}_R, \lambda_{\tilde{B}'}, \tilde{B}) &= \frac{g_3 g_1(g_{YB} + g_B)}{6M_{SUSY}} \sqrt{x_d x_{BB'} x_{\mu_H}} e^{i\theta_{BB'}} e^{i\theta_{\mu_H}} \tan \beta \\
&\quad \times [\sqrt{x_1 x_{\lambda_{\tilde{B}'}}} f(x_{BB'}, x_1, x_{\tilde{d}_L}^0, x_{\tilde{d}_R}^0) - g(x_{BB'}, x_1, x_{\tilde{d}_L}, x_{\tilde{d}_R})].
\end{aligned} \tag{38}$$

e. The one-loop contributions to the quark EDMs and CEDMs from $\tilde{B}-\lambda_{\tilde{B}'}-\tilde{d}_L-\tilde{d}_R$.

$$\begin{aligned}
d_q^{\gamma(e)}(\tilde{d}_L, \tilde{d}_R, \tilde{B}, \lambda_{\tilde{B}'}) &= -\frac{eg_1(-2g_{YB} + g_B)}{36M_{SUSY}} \sqrt{x_d x_{BB'} x_{\mu_H}} e^{i\theta_{BB'}} e^{i\theta_{\mu_H}} \tan \beta \\
&\quad \times [\sqrt{x_1 x_{\tilde{B}'}} f(x_{BB'}, x_1, x_{\tilde{d}_L}, x_{\tilde{d}_R}) - g(x_{BB'}, x_1, x_{\tilde{d}_L}, x_{\tilde{d}_R})]; \\
d_q^{g(e)}(\tilde{d}_L, \tilde{d}_R, \tilde{B}, \lambda_{\tilde{B}'}) &= \frac{g_3 g_1(-2g_{YB} + g_B)}{12M_{SUSY}} \sqrt{x_d x_{BB'} x_{\mu_H}} e^{i\theta_{BB'}} e^{i\theta_{\mu_H}} \tan \beta \\
&\quad \times [\sqrt{x_1 x_{\tilde{B}'}} f(x_{BB'}, x_1, x_{\tilde{d}_L}, x_{\tilde{d}_R}) - g(x_{BB'}, x_1, x_{\tilde{d}_L}, x_{\tilde{d}_R})], \tag{39}
\end{aligned}$$

f. The one-loop contributions to the quark EDMs and CEDMs from $\tilde{W}^0-\tilde{H}^0-\tilde{d}_L$.

$$\begin{aligned}
d_q^{\gamma(f)}(\tilde{d}_L, \tilde{H}^0, \tilde{W}^0) &= \frac{eg_2^2}{6M_{SUSY}} \sqrt{x_2 x_d x_{\mu_H}} e^{i\theta_2} e^{i\theta_{\mu_H}} \tan \beta I_2(x_2, x_{\mu_H}, x_{\tilde{d}_L}); \\
d_q^{g(f)}(\tilde{d}_L, \tilde{H}^0, \tilde{W}^0) &= -\frac{g_3 g_2^2}{2M_{SUSY}} \sqrt{x_2 x_d x_{\mu_H}} e^{i\theta_2} e^{i\theta_{\mu_H}} \tan \beta I_2(x_2, x_{\mu_H}, x_{\tilde{d}_L}). \tag{40}
\end{aligned}$$

g. The one-loop contributions to the quark EDMs and CEDMs from $\tilde{W}^\pm-\tilde{H}^\pm-\tilde{u}_L$.

$$\begin{aligned}
d_q^{\gamma(g)}(\tilde{u}_L, \tilde{W}^\pm, \tilde{H}^\pm) &= \frac{eg_2^2}{M_{SUSY}} \sqrt{x_2 x_u x_{\mu_H}} e^{i\theta_2} e^{i\theta_{\mu_H}} \tan \beta \left\{ \frac{2}{3} I_5(x_2, x_{\mu_H}, x_{\tilde{u}_L}) + \frac{1}{4} I_4(x_2, x_{\mu_H}, x_{\tilde{u}_L}^0) \right\}; \\
d_q^{g(g)}(\tilde{u}_L, \tilde{W}^\pm, \tilde{H}^\pm) &= \frac{2g_3 g_2^2}{M_{SUSY}} \sqrt{x_2 x_u x_{\mu_H}} e^{i\theta_2} e^{i\theta_{\mu_H}} \tan \beta I_5(x_{\tilde{u}_L}, x_2, x_{\mu_H}). \tag{41}
\end{aligned}$$

The functions $I_4(x, y, z)$, $I_5(x, y, z)$ are defined as

$$\begin{aligned}
I_4(x, y, z) &= \frac{1}{32\pi^2} \left\{ \frac{2x(2x^3 y + x^2(x-5y)z + y(x+y)z^2) \log x}{(x-y)^3(x-z)^3} \right. \\
&\quad - \frac{2y(2xy^3 + y^2(-5x+y)z + x(x+y)z^2) \log y}{(x-y)^3(y-z)^3} \\
&\quad - \frac{2x^2 y^2(x+y) - xy(5x^2 + 2xy + 5y^2)z + (x+y)(x^2 + 4xy + y^2)z^2 + (x^2 - 6xy + y^2)z^3}{(x-y)^2(x-z)^2(y-z)^2} \\
&\quad \left. + \frac{2z^2(xy(x+y) - 4xyz + (x+y)z^2) \log z}{(x-z)^3(z-y)^3} \right\}; \tag{42}
\end{aligned}$$

$$\begin{aligned}
I_5(x, y, z) &= \frac{1}{16\pi^2} \left\{ \frac{x^2 \log x}{(y-x)(x-z)^2} + \frac{y^2 \log y}{(x-y)(y-z)^2} - \frac{z[2xy - z(x+y)] \log z}{(x-z)^2(y-z)^2} \right. \\
&\quad \left. + \frac{z}{(x-z)(z-y)} \right\}. \tag{43}
\end{aligned}$$

h. The one-loop contributions to the quark EDMs and CEDMs from $\lambda_{\tilde{g}}-\tilde{d}_L-\tilde{d}_R$.

$$\begin{aligned}
d_l^{\gamma(h)}(\tilde{d}_L, \tilde{d}_R, \lambda_{\tilde{g}}) &= \frac{e}{18M_{SUSY}} \sqrt{x_d x_{\mu_H} x_{\lambda_{\tilde{g}}}} e^{i\theta_{\mu_H}} e^{i\theta_g} \tan \beta I_1(x_{\lambda_{\tilde{g}}}, x_{\tilde{d}_L}, x_{\tilde{d}_R}); \\
d_l^{g(h)}(\tilde{d}_L, \tilde{d}_R, \lambda_{\tilde{g}}) &= -\frac{g_3}{M_{SUSY}} \sqrt{x_d x_{\mu_H} x_{\lambda_{\tilde{g}}}} e^{i\theta_{\mu_H}} e^{i\theta_g} \tan \beta \\
&\quad \times \left[\frac{1}{6} I_1(x_{\lambda_{\tilde{g}}}, x_{\tilde{d}_L}, x_{\tilde{d}_R}) + \frac{3}{2} I_6(x_{\lambda_{\tilde{g}}}, x_{\tilde{d}_L}, x_{\tilde{d}_R}) \right]. \tag{44}
\end{aligned}$$

The function $I_6(x, y, z)$ is defined as

$$I_6(x, y, z) = \frac{1}{32\pi^2} \left\{ -\frac{2[x^2(x^2 - xy + y^2) - xyz(x + y) + y^2z^2] \log x}{(x - y)^3(x - z)^3} - \frac{2[x^2y - xz(y + z) + yz^2] \log z}{(x - z)^3(y - z)^2} + \frac{2y[x^2 - 2xy + y(2y - z)] \log y}{(x - y)^3(y - z)^2} - \frac{2x^3 - x^2(5y + z) + x(y^2 + 4yz + z^2) + yz(y - 3z)}{(x - y)^2(x - z)^2(y - z)} \right\}. \quad (45)$$

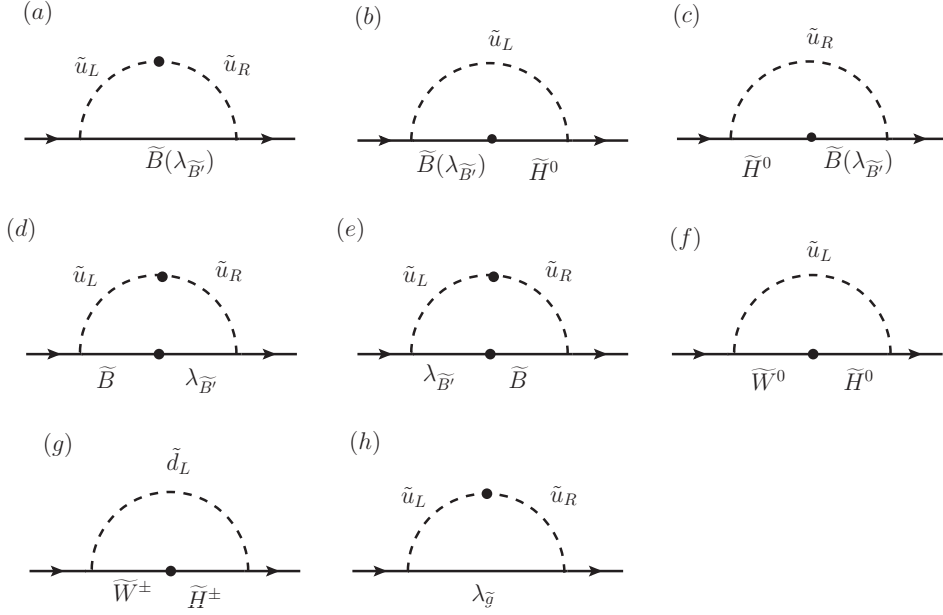


FIG. 3: Feynman diagrams of up-quark for generating neutron EDM based on MIA. External photons connect to charged internal lines in all possible ways, while external gluons connect to colored internal lines.

A. The one-loop contributions to the quark EDMs and CEDMs from \tilde{B} - \tilde{u}_L - \tilde{u}_R .

$$d_g^{\gamma(A)}(\tilde{u}_L, \tilde{u}_R, \tilde{B}) = -\frac{4eg_1^2}{27M_{SUSY}} \sqrt{x_1 x_u x_{\mu H}} e^{i\theta_1} e^{i\theta_{\mu H}} I_1(x_1, x_{\tilde{u}_L}, x_{\tilde{u}_R});$$

$$d_g^{g(A)}(\tilde{u}_L, \tilde{u}_R, \tilde{B}) = \frac{4g_3g_1^2}{9M_{SUSY}} \sqrt{x_1 x_u x_{\mu H}} e^{i\theta_1} e^{i\theta_{\mu H}} I_1(x_1, x_{\tilde{u}_L}, x_{\tilde{u}_R}). \quad (46)$$

The one-loop contributions to the quark EDMs and CEDMs from $\lambda_{\tilde{B}'}$ - \tilde{u}_L - \tilde{u}_R .

$$d_g^{\gamma(A)}(\tilde{u}_L, \tilde{u}_R, \lambda_{\tilde{B}'}) = -\frac{e(g_{YB} + g_B)(4g_{YB} + g_B)}{27M_{SUSY}} \sqrt{x_{\lambda_{\tilde{B}'}} x_u x_{\mu H}} e^{i\theta_1} e^{i\theta_{\mu H}} I_1(x_{\lambda_{\tilde{B}'}} , x_{\tilde{u}_L}, x_{\tilde{u}_R});$$

$$d_g^{g(A)}(\tilde{u}_L, \tilde{u}_R, \lambda_{\tilde{B}'}) = \frac{g_3(g_{YB} + g_B)(4g_{YB} + g_B)}{9M_{SUSY}} \sqrt{x_{\lambda_{\tilde{B}'}} x_u x_{\mu H}} e^{i\theta_1} e^{i\theta_{\mu H}} I_1(x_{\lambda_{\tilde{B}'}} , x_{\tilde{u}_L}, x_{\tilde{u}_R}). \quad (47)$$

B. The one-loop contributions to the quark EDMs and CEDMs from $\tilde{B}-\tilde{H}^0-\tilde{u}_L$.

$$\begin{aligned} d_l^{\gamma(B)}(\tilde{u}_L, \tilde{H}^0, \tilde{B}) &= -\frac{eg_1^2}{9M_{SUSY}}\sqrt{x_1x_u x_{\mu H}}e^{i\theta_1}e^{i\theta_{\mu H}}I_2(x_1, x_{\mu H}, x_{\tilde{u}_L}); \\ d_l^{g(B)}(\tilde{u}_L, \tilde{H}^0, \tilde{B}) &= \frac{g_3g_1^2}{3M_{SUSY}}\sqrt{x_1x_u x_{\mu H}}e^{i\theta_1}e^{i\theta_{\mu H}}I_2(x_1, x_{\mu H}, x_{\tilde{u}_L}). \end{aligned} \quad (48)$$

The one-loop contributions to the quark EDMs and CEDMs from $\lambda_{\tilde{B}'}-\tilde{H}^0-\tilde{u}_L$.

$$\begin{aligned} d_l^{\gamma(B)}(\tilde{u}_L, \tilde{H}^0, \lambda_{\tilde{B}'}) &= \frac{eg_1(g_{YB} + g_B)}{9M_{SUSY}}\sqrt{x_{\lambda_{\tilde{B}'}}x_u x_{\mu H}}e^{i\theta_1}e^{i\theta_{\mu H}}I_2(x_{\lambda_{\tilde{B}'}} , x_{\mu H}, x_{\tilde{u}_L}); \\ d_l^{g(B)}(\tilde{u}_L, \tilde{H}^0, \lambda_{\tilde{B}'}) &= -\frac{g_3g_1(g_{YB} + g_B)}{3M_{SUSY}}\sqrt{x_{\lambda_{\tilde{B}'}}x_u x_{\mu H}}e^{i\theta_1}e^{i\theta_{\mu H}}I_2(x_{\lambda_{\tilde{B}'}} , x_{\mu H}, x_{\tilde{u}_L}). \end{aligned} \quad (49)$$

C. The one-loop contributions to the quark EDMs and CEDMs from $\tilde{B}-\tilde{H}^0-\tilde{u}_R$.

$$\begin{aligned} d_l^{\gamma(C)}(\tilde{u}_R, \tilde{H}^0, \tilde{B}) &= -\frac{4eg_1^2}{9M_{SUSY}}\sqrt{x_1x_u x_{\mu H}}e^{i\theta_1}e^{i\theta_{\mu H}}I_2(x_1, x_{\mu H}, x_{\tilde{u}_R}); \\ d_l^{g(C)}(\tilde{u}_R, \tilde{H}^0, \tilde{B}) &= \frac{4g_3g_1^2}{3M_{SUSY}}\sqrt{x_1x_u x_{\mu H}}e^{i\theta_1}e^{i\theta_{\mu H}}I_2(x_1, x_{\mu H}, x_{\tilde{u}_R}). \end{aligned} \quad (50)$$

The one-loop contributions to the quark EDMs and CEDMs from $\lambda_{\tilde{B}'}-\tilde{H}^0-\tilde{u}_R$.

$$\begin{aligned} d_l^{\gamma(C)}(\tilde{u}_R, \tilde{H}^0, \lambda_{\tilde{B}'}) &= \frac{eg_1(g_{YB} + g_B)}{9M_{SUSY}}\sqrt{x_{\lambda_{\tilde{B}'}}x_u x_{\mu H}}e^{i\theta_1}e^{i\theta_{\mu H}}I_2(x_{\lambda_{\tilde{B}'}} , x_{\mu H}, x_{\tilde{u}_R}); \\ d_l^{g(C)}(\tilde{u}_R, \tilde{H}^0, \lambda_{\tilde{B}'}) &= -\frac{g_3g_1(g_{YB} + g_B)}{3M_{SUSY}}\sqrt{x_{\lambda_{\tilde{B}'}}x_u x_{\mu H}}e^{i\theta_1}e^{i\theta_{\mu H}}I_2(x_{\lambda_{\tilde{B}'}} , x_{\mu H}, x_{\tilde{u}_R}). \end{aligned} \quad (51)$$

D. The one-loop contributions to the quark EDMs and CEDMs from $\lambda_{\tilde{B}'}-\tilde{B}-\tilde{u}_L-\tilde{u}_R$.

$$\begin{aligned} d_l^{\gamma(D)}(\tilde{u}_L, \tilde{u}_R, \lambda_{\tilde{B}'}, \tilde{B}) &= \frac{2eg_1(g_{YB} + g_B)}{9M_{SUSY}}\sqrt{x_d x_{BB'} x_{\mu H}}e^{i\theta_{BB'}}e^{i\theta_{\mu H}} \\ &\quad \times [\sqrt{x_1 x_{\lambda_{\tilde{B}'}}}f(x_{BB'}, x_1, x_{\tilde{u}_L}, x_{\tilde{u}_R}) - g(x_{BB'}, x_1, x_{\tilde{u}_L}, x_{\tilde{u}_R})]; \\ d_l^{g(D)}(\tilde{u}_L, \tilde{u}_R, \lambda_{\tilde{B}'}, \tilde{B}) &= -\frac{2g_3g_1(g_{YB} + g_B)}{3M_{SUSY}}\sqrt{x_d x_{BB'} x_{\mu H}}e^{i\theta_{BB'}}e^{i\theta_{\mu H}} \\ &\quad \times [\sqrt{x_1 x_{\lambda_{\tilde{B}'}}}f(x_{BB'}, x_1, x_{\tilde{u}_L}, x_{\tilde{u}_R}) - g(x_{BB'}, x_1, x_{\tilde{u}_L}, x_{\tilde{u}_R})]. \end{aligned} \quad (52)$$

E. The one-loop contributions to the quark EDMs and CEDMs from $\tilde{B}-\lambda_{\tilde{B}'}-\tilde{u}_L-\tilde{u}_R$.

$$\begin{aligned} d_l^{\gamma(E)}(\tilde{u}_L, \tilde{u}_R, \lambda_{\tilde{B}'}, \tilde{B}) &= \frac{2eg_1(4g_{YB} + g_B)}{9M_{SUSY}}\sqrt{x_d x_{BB'} x_{\mu H}}e^{i\theta_{BB'}}e^{i\theta_{\mu H}} \\ &\quad \times [\sqrt{x_1 x_{B'}}f(x_{BB'}, x_1, x_{\tilde{u}_L}, x_{\tilde{u}_R}) - g(x_{BB'}, x_1, x_{\tilde{u}_L}, x_{\tilde{u}_R})]; \\ d_l^{g(E)}(\tilde{u}_L, \tilde{u}_R, \lambda_{\tilde{B}'}, \tilde{B}) &= -\frac{2g_3g_1(4g_{YB} + g_B)}{3M_{SUSY}}\sqrt{x_d x_{BB'} x_{\mu H}}e^{i\theta_{BB'}}e^{i\theta_{\mu H}} \\ &\quad \times [\sqrt{x_1 x_{B'}}f(x_{BB'}, x_1, x_{\tilde{u}_L}, x_{\tilde{u}_R}) - g(x_{BB'}, x_1, x_{\tilde{u}_L}, x_{\tilde{u}_R})]. \end{aligned} \quad (53)$$

F. The one-loop contributions to the quark EDMs and CEDMs from \widetilde{W}^0 - \widetilde{H}^0 - \widetilde{u}_L .

$$\begin{aligned} d_l^{\gamma(F)}(\widetilde{u}_L, \widetilde{H}^0, \widetilde{W}^0) &= \frac{eg_2^2}{3M_{SUSY}} \sqrt{x_2 x_u x_{\mu_H}} e^{i\theta_2} e^{i\theta_{\mu_H}} I_2(x_2, x_{\mu_H}, x_{\widetilde{u}_L}); \\ d_l^{g(F)}(\widetilde{u}_L, \widetilde{H}^0, \widetilde{W}^0) &= -\frac{g_3 g_2^2}{M_{SUSY}} \sqrt{x_2 x_u x_{\mu_H}} e^{i\theta_2} e^{i\theta_{\mu_H}} I_2(x_2, x_{\mu_H}, x_{\widetilde{u}_L}). \end{aligned} \quad (54)$$

G. The one-loop contributions to the quark EDMs and CEDMs from \widetilde{W}^\pm - \widetilde{H}^\pm - \widetilde{d}_L .

$$\begin{aligned} d_l^{\gamma(G)}(\widetilde{d}_L, \widetilde{W}^\pm, \widetilde{H}^\pm) &= \frac{eg_2^2}{2M_{SUSY}} \sqrt{x_2 x_d x_{\mu_H}} e^{i\theta_2} e^{i\theta_{\mu_H}} \left\{ \frac{2}{3} I_5(x_2, x_{\mu_H}, x_{\widetilde{d}_L}) \right. \\ &\quad \left. + \frac{1}{4} I_4(x_2, x_{\mu_H}, x_{\widetilde{d}_L}) \right\}; \\ d_l^{g(G)}(\widetilde{d}_L, \widetilde{W}^\pm, \widetilde{H}^\pm) &= \frac{g_3 g_2^2}{M_{SUSY}} \sqrt{x_2 x_d x_{\mu_H}} e^{i\theta_2} e^{i\theta_{\mu_H}} I_5(x_{\widetilde{d}_L}, x_2, x_{\mu_H}). \end{aligned} \quad (55)$$

H. The one-loop contributions to the quark EDMs and CEDMs from $\lambda_{\widetilde{g}}$ - \widetilde{u}_L - \widetilde{u}_R .

$$\begin{aligned} d_l^{\gamma(H)}(\widetilde{u}_L, \widetilde{u}_R, \lambda_{\widetilde{g}}) &= \frac{2e}{18M_{SUSY}} \sqrt{x_u x_{\mu_H} x_{\lambda_{\widetilde{g}}}} e^{i\theta_{\mu_H}} e^{i\theta_3} I_1(x_{\lambda_{\widetilde{g}}}, x_{\widetilde{u}_L}, x_{\widetilde{u}_R}); \\ d_l^{g(H)}(\widetilde{u}_L, \widetilde{u}_R, \lambda_{\widetilde{g}}) &= -\frac{2g_3}{M_{SUSY}} \sqrt{x_u x_{\mu_H} x_{\lambda_{\widetilde{g}}}} e^{i\theta_{\mu_H}} e^{i\theta_3} \left\{ \frac{1}{6} I_1(x_{\lambda_{\widetilde{g}}}, x_{\widetilde{u}_L}, x_{\widetilde{u}_R}) \right. \\ &\quad \left. + \frac{3}{2} I_6(x_{\lambda_{\widetilde{g}}}, x_{\widetilde{u}_L}, x_{\widetilde{u}_R}) \right\}. \end{aligned} \quad (56)$$

The parameter is defined as follows

$$m_g = M_3 * e^{i*\theta_3}. \quad (57)$$

The Wilson coefficient of the purely gluonic Weinberg operator originates from the two-loop "gluino-squark" diagrams, and the concrete expression of C_5 can be written as

$$\begin{aligned} C_5(\Lambda) &= -\frac{3g_3^5}{(4\pi)^4 M_3^3} \left\{ m_t \mathfrak{S} \left[e^{2i\theta_3} (Z_{\widetilde{t}})_{2,2} (Z_{\widetilde{t}})_{2,1}^\dagger \right] \frac{x_{\widetilde{t}_1} - x_{\widetilde{t}_2}}{x_{M_3}} H \left(\frac{x_{\widetilde{t}_1}}{x_{M_3}}, \frac{x_{\widetilde{t}_2}}{x_{M_3}}, \frac{x_t}{x_{M_3}} \right) \right. \\ &\quad \left. + m_b \mathfrak{S} \left[e^{2i\theta_3} (Z_{\widetilde{b}})_{2,2} (Z_{\widetilde{b}})_{2,1}^\dagger \right] \frac{x_{\widetilde{b}_1} - x_{\widetilde{b}_2}}{x_{M_3}} H \left(\frac{x_{\widetilde{b}_1}}{x_{M_3}}, \frac{x_{\widetilde{b}_2}}{x_{M_3}}, \frac{x_b}{x_{M_3}} \right) \right\}, \end{aligned} \quad (58)$$

The explicit expression for the function $H(x, y, z)$ can be found in Ref [34]. The results obtained at the matching scale Λ should be transformed down to the chirality breaking scale Λ_χ . So the renormalization group equations (RGEs) for the Wilson coefficients of the Weinberg operator and the quark EDMs, CEDMs should be solved. The relations between the results at two different scales Λ and Λ_χ are presented here.

$$d_q^\gamma(\Lambda_\chi) = 1.53 d_q^\gamma(\Lambda), \quad d_q^g(\Lambda_\chi) = 3.4 d_q^g(\Lambda), \quad C_5(\Lambda_\chi) = 3.4 C_5(\Lambda) \quad (59)$$

There are three type contributions to the quark EDM, 1 the electroweak contribution d_q^γ , 2 the CEDM contribution d_q^g , 3 the Weinberg operator contribution. Each type contribution can be calculated numerically. At a low scale, the quark EDM can be obtained from d_q^γ , d_q^g and $C_5(\Lambda_\chi)$ by the following formula[35]

$$d_q = d_q^\gamma(\Lambda_\chi) + \frac{e}{4\pi} d_q^g(\Lambda_\chi) + \frac{e\Lambda_\chi}{4\pi} C_5(\Lambda_\chi) \quad (60)$$

From the quark model, the EDM of neutron is derived from up-quark EDM d_u and down-quark EDM d_d with the following expression

$$d_n = \frac{1}{3}(4d_d - d_u) \quad (61)$$

IV. NUMERICAL ANALYSIS

In this work to obtain the numerical results, the relevant parameters are shown here.

$\tan \beta = 10$, $g_{YB} = -0.2$, $g_B = 0.3$, $v_\eta = 12$ TeV, $v_{\bar{\eta}} = 12$ TeV, $v_S = 2$ TeV, $\lambda = 0.25$, $M_{susy} = 1500$ GeV, $m_{W0} = 900$ GeV, $m_g = 2500$ GeV, $m_B = 1200$ GeV, $m_{u_L} = 1800$ GeV, $m_{u_R} = 2000$ GeV, $m_{d_R} = 1900$ GeV, $m_{\lambda_{\bar{B}'}} = 3000$ GeV.

A. Numerical analysis for lepton EDM

Leptons are elementary particles. Their EDMs directly characterize CP violation effects in fundamental interactions and strongly depend on the lepton masses. The τ -lepton, the heaviest lepton, is most sensitive to CP violation. The electron, the lightest lepton, has an extremely weak EDM signal that requires complex detection. The μ -lepton resides in the intermediate response range. By adopting the MIA, the EDM can be expressed as an analytical combination of various mass insertion parameters and the imaginary parts of CP-violating phases. Thus, it shows clear parametric responses to gauge coupling constants g_{YB} , g_B , the Higgs vacuum structure $\tan \beta$, and independent CP phases θ_{μ_H} , θ_1 .

1. The tau EDM

Fig.4 (a) shows the variation of $|d_\tau|$ with g_{YB} for different values of $\tan \beta$. The phase $\theta_{\mu_H} = \frac{\pi}{3}$ and other phases $\theta_1 = \theta_2 = \theta_{1'} = \theta_{BB'} = 0$. In the range of $0 \leq g_{YB} \leq 0.60$, d_τ

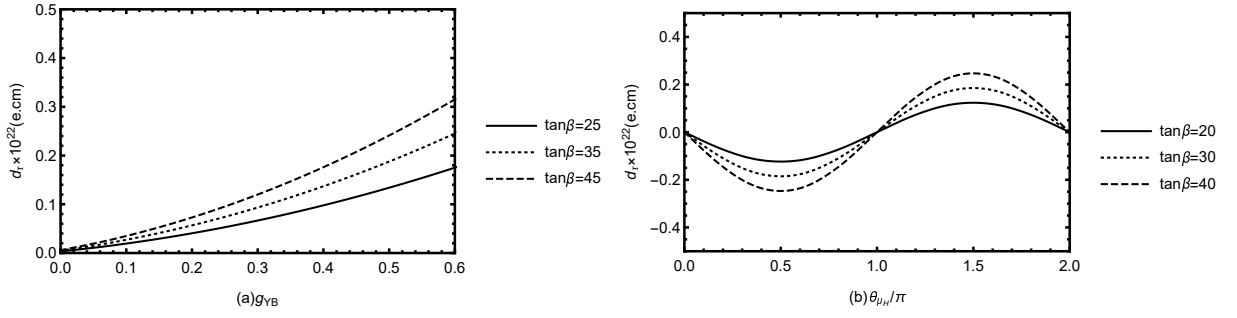


FIG. 4: The effects of g_{YB} , $\theta_{\mu H}$ and $\tan\beta$ on d_τ .

exhibits an approximately linear increase with g_{YB} , indicating that this gauge interaction has an enhancing effect on the EDM of the τ lepton. At the same value of g_{YB} , increasing $\tan\beta$ leads to an overall increase in d_τ . Fig.4 (b) presents the variation of d_τ with $\theta_{\mu H}$ for different $\tan\beta$. Other phases $\theta_1 = \theta_2 = \theta_{1'} = \theta_{BB'} = 0$. d_τ undergoes a standard sinusoidal oscillation with a period of 2π as $\theta_{\mu H}$ varies, with zeros located at $\theta_{\mu H} = 0, \pi, 2\pi$. As $\tan\beta$ increases, the oscillation amplitude increases significantly while the zero-crossing positions remain unchanged. This indicates that $\tan\beta$ does not change the phase structure, but only affects the weight of the phase term in the total amplitude. $\theta_{\mu H}$ provides a new CP-violating source independent of the CKM phase in the SM. The obtained values of d_τ are consistent with the current experimental constraints, being approximately three orders of magnitude lower than the experimental upper limit.

2. The muon EDM

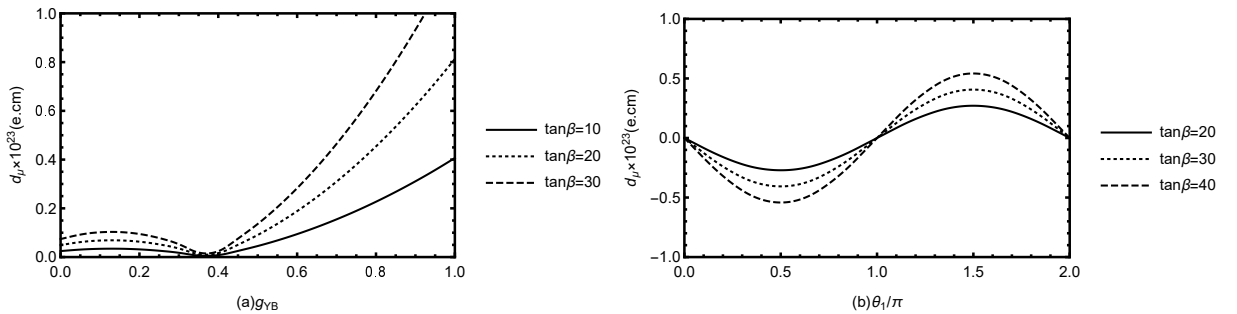


FIG. 5: The effects of g_{YB} , θ_1 and $\tan\beta$ on d_μ .

Fig.5 (a) illustrates the variation of $|d_\mu|$ with g_{YB} for different values of $\tan\beta$. Phase

$\theta_{\mu H} = \frac{\pi}{3}$ and other phases $\theta_1 = \theta_2 = \theta_{\mu H} = \theta_{1'} = \theta_{BB'} = 0$. In the range of $0 \leq g_{YB} \leq 1.0$, $|d_\mu|$ first increases slightly and then decreases to zero as g_{YB} increases. This indicates that there exists a mutual cancellation effect between the contributions of different loop diagrams within this parameter range. When $g_{YB} \in [0.4, 1.0]$, $|d_\mu|$ resumes a monotonically increasing trend, and the growth rate accelerates with the increase of $\tan \beta$. Fig.5 (b) depicts the variation behavior of d_μ with the phase θ_1 for $\tan \beta = 20, 30, 40$. Other phase $\theta_2 = \theta_{\mu H} = \theta_{1'} = \theta_{BB'} = 0$. Similar to the case of the τ lepton, d_μ exhibits a typical sinusoidal oscillation with a period of 2π as θ_1 varies, where the oscillation zeros correspond to $\theta_1 = 0, \pi, 2\pi$. This reflects the periodic dependence of this CP-violating phase in amplitude interference. With the increase of $\tan \beta$, the oscillation amplitude is significantly enhanced. This demonstrates that $\tan \beta$ does not alter the phase structure itself, but rather enhances the observable strength of the CP-violating effect by boosting the relevant Yukawa couplings. As a CP-violating source independent of the CKM phase in the Standard Model, the considerable signal induced by θ_1 in the lepton electric dipole moment provides a promising avenue for probing new physics CP phases in higher-precision experiments.

3. The electron EDM

The experimental upper limit on the electron EDM (d_e) is very strict. To ensure that the predicted d_e values from the N-B-LSSM within the framework of the MIA satisfy this constraint, three commonly used suppression methods are adopted as follows: 1. Adopting small CP-violating phases; 2. Increasing the masses of relevant new particles to suppress loop amplitudes; 3. Exploiting internal cancellations among contributions from distinct phases, thereby reducing the imaginary part contributions without violating the phase structure.

a. small CP-violating phase Fig.6 depicts the behavior of the electron EDM $|d_e|$ under the small CP-violating phase. In this case $\theta_{1'} = \frac{\pi}{1000}$, other phases $\theta_1 = \theta_2 = \theta_{\mu H} = \theta_{BB'} = 0$. In the figure, as g_B increases from 0 to approximately 0.6, $|d_e|$ decreases monotonically and reaches a minimum at $g_B \approx 0.6$. This indicates that the increase in g_B changes the relative weights of the various loop contribution terms, thereby suppressing the net imaginary part $|d_e|$ within this region. Beyond $g_B \approx 0.6$, $|d_e|$ increases significantly, demonstrating that g_B has a crucial influence on $|d_e|$ in the small phase angle limit. Different values of $\tan \beta$ (8, 10, 12) only scale the overall amplitude of $|d_e|$ at each g_B , without changing the overall trend.

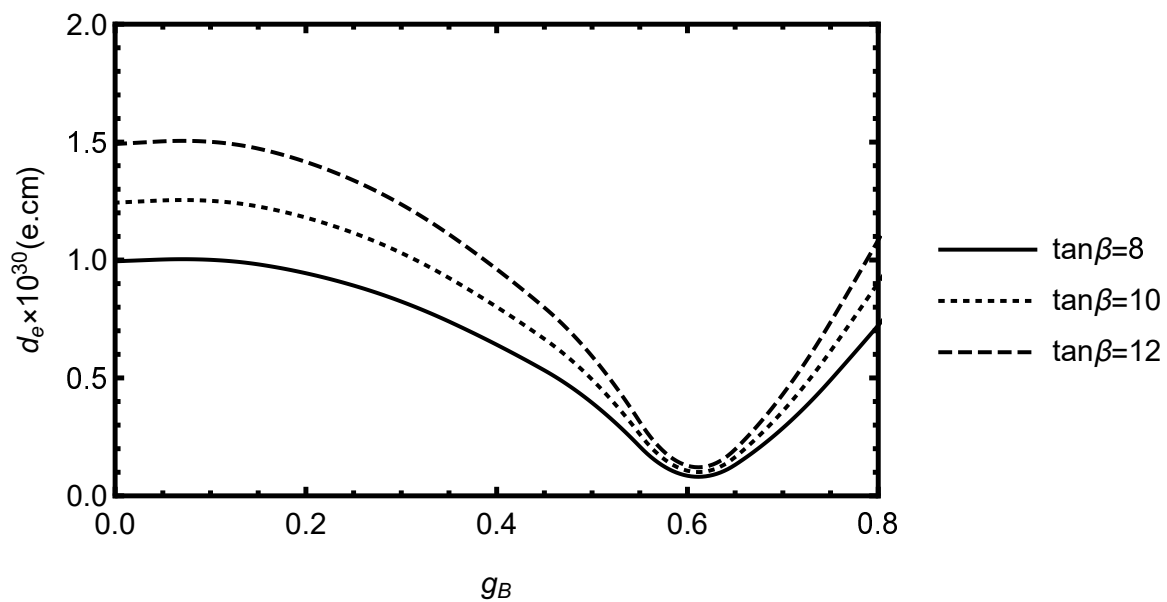


FIG. 6: The effects of g_B and $\tan\beta$ on d_e .

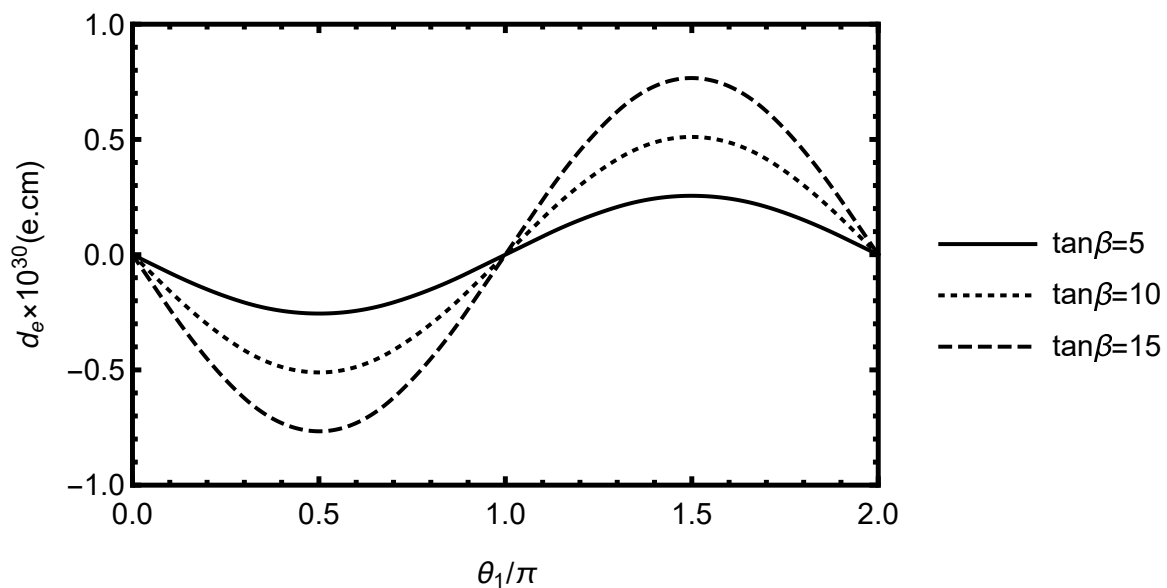


FIG. 7: The effects of θ_1 and $\tan\beta$ on d_e .

b. large-mass approach In Fig.7, we calculate with the large-mass approach ($m_{\tilde{e}_L} = 13000$ GeV, $m_{\tilde{e}_R} = 14000$ GeV) for $\tan\beta = 5, 10,$ and 15 . The phase $\theta_2 = \theta_{\mu_H} = \theta_{1'} = \theta_{BB'} = 0$. The electron EDM d_e still exhibits sinusoidal oscillations with a 2π period as a function of θ_1 , consistent with the patterns observed for the τ -lepton and μ -lepton. However, the oscillation amplitude is extremely small. Heavy lepton partners only reduce the magnitude of d_e without destroying the phase effect. Particle masses within the 10

TeV range combined with a normal phase can satisfy the experimental constraints on d_e . Nevertheless, this violates the principle of naturalness.

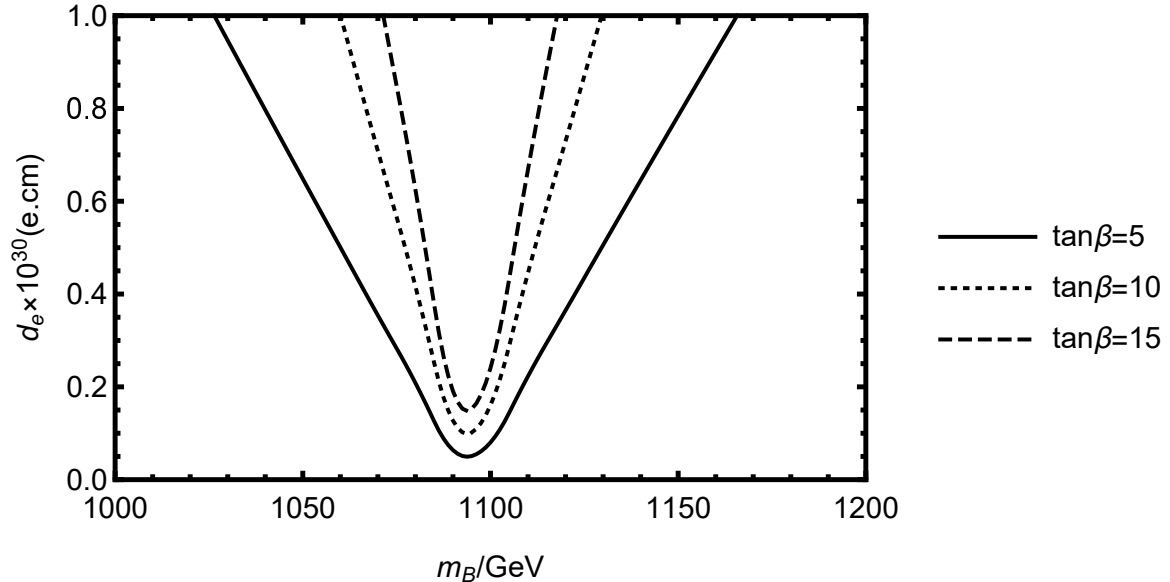


FIG. 8: The effects of m_B and $\tan \beta$ on d_e .

c. the phase cancellation mechanism In Fig.8, we introduce the phase cancellation mechanism and scan the mass parameter m_B . In this case, the phase $\theta_1 = \frac{\pi}{20}$, $\theta_{1'} = \frac{\pi}{20}$, $\theta_2 = \theta_{\mu_H} = \theta_{BB'} = 0$. d_e shows a clear V-shaped distribution, with a near-zero optimal cancellation point appearing around $m_B \simeq 1100$ GeV. As $\tan \beta$ decreases, the V-shaped structure generally becomes deeper and wider. This means $\tan \beta$ raises the weight of phase-related terms in the total amplitude. It can be seen that this possible method has CP-violating phases of normal size, and the particle masses are in the TeV range. The results obtained are also more likely to meet the experimental limits.

B. Numerical analysis for neutron EDM

Compared to the lepton EDM, the neutron EDM originates from CP violation effects and chiral structures at a more fundamental quark level, exhibiting richer nonlinear dependencies on model parameters.

In Fig.9 (a), the neutron EDM $|d_n|$ exhibits a monotonically decreasing trend as the new baryon mass m_B increases. The phases $\theta_2 = \theta_3 = \theta_{\mu_H} = \theta_{1'} = \theta_{BB'} = 0$. The CP-violating phase θ_1 only regulates the amplitude of d_n without altering its overall evolutionary behavior

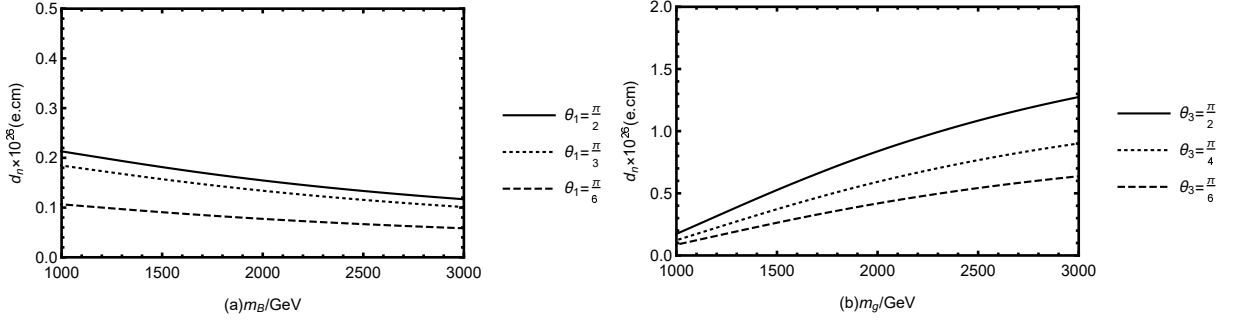


FIG. 9: The effects of m_B and θ_1 on d_n , m_g and θ_3 on d_n .

of decreasing with m_B . In the low-mass region ($m_B \lesssim 1500$ GeV), $|d_n|$ shows significant sensitivity to the variation of m_B , decreasing rapidly with increasing mass; after entering the high-mass region ($m_B \gtrsim 2000$ GeV), the decreasing trend gradually slows down. This behavior reflects that the contribution of heavy particles to loop propagators becomes stable as their mass increases. Figure 9(b) shows the dependence of the neutron EDM $|d_n|$ on the gluino mass $m_{\tilde{g}}$ (1000-3000 GeV) for different CP-violating phases $\theta_3 = \pi/2, \pi/4, \pi/6$. The other CP phases are set to zero ($\theta_1 = \theta_2 = \theta_{\mu H} = \theta_{1'} = \theta_{BB'} = 0$). The results indicate that $|d_n|$ increases monotonically with $m_{\tilde{g}}$, with the dominant contribution arising from the imaginary part of $m_{\tilde{g}}e^{i\theta_3}$. As $m_{\tilde{g}}$ and θ_3 increase, this imaginary part grows, driving the rise in $|d_n|$. However, in the region $m_{\tilde{g}} > 2000$ GeV, this growth trend is suppressed. This further highlights the combined role of the phase θ_3 as the primary source of CP violation and the mass $m_{\tilde{g}}$ in modulating this correction effect. The synergistic effect between the gluino mass $m_{\tilde{g}}$ and θ_3 can effectively enhance the magnitude of the EDM contribution, playing an important role in ensuring that d_n satisfies experimental constraints within the N-B-LSSM.

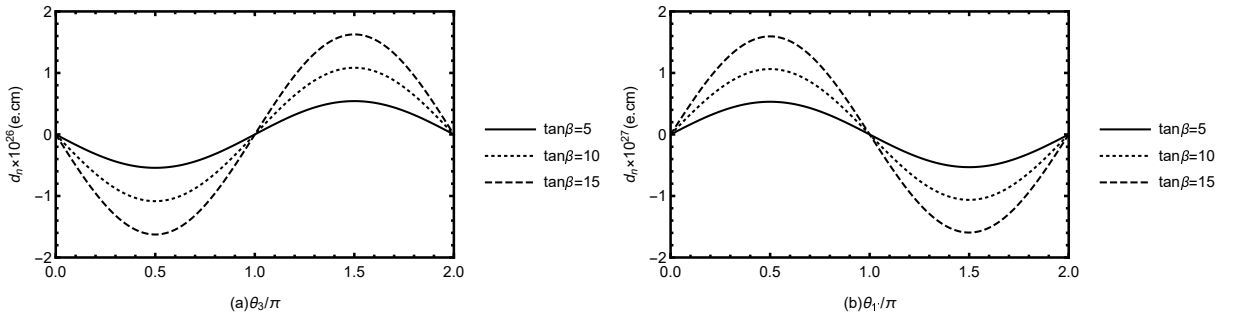


FIG. 10: The effects of θ_3 and $\tan \beta$ on d_n , $\theta_{B'}$ and $\tan \beta$ on d_n .

Fig.10 (a) illustrates the variation of the $d_n \times 10^{26}$ e·cm with the CP-violating phase θ_3 for different values of $\tan \beta = 5, 10, 15$. The phases $\theta_1 = \theta_2 = \theta_{\mu H} = \theta_{1'} = \theta_{BB'} = 0$. d_n exhibits an oscillatory behavior with a period of 2π as θ_3 varies, with zeros precisely at $\theta_3 = 0, \pi, 2\pi$, where the CP-violating effects are completely cancelled. A larger value of $\tan \beta$ leads to a more significant oscillation amplitude, indicating that it has a stable amplifying effect on this CP-violating interference effect. In Fig.10(b), the peak and valley positions of the neutron EDM d_n oscillating with the CP-violating phase $\theta_{1'}$ are exactly opposite to the oscillation trajectory regulated by θ_3 in Fig.9(a), and its oscillation amplitude is slightly lower than that in the case dominated by θ_3 . In this case, the phases $\theta_1 = \theta_2 = \theta_{\mu H} = \theta_3 = \theta_{BB'} = 0$. This indicates that $\theta_{1'}$ is another CP-violating source independent of θ_3 , with a contribution strength weaker than θ_3 .

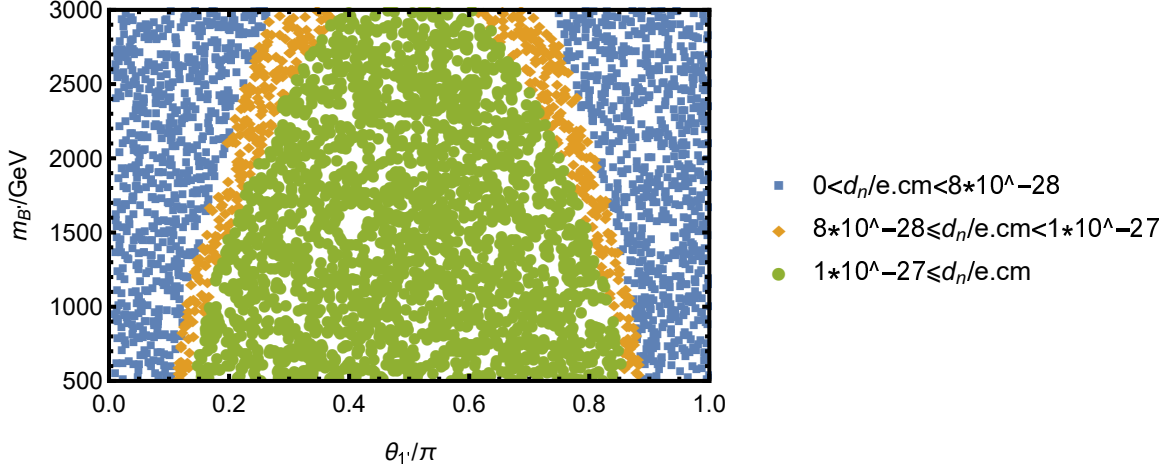


FIG. 11: The effects of $m_{B'}$ and $\theta_{1'}$ on d_n .

In the N-B-LSSM, we scan the parameter space of the B' boson mass $m_{B'}$ (500 GeV-3000 GeV) and the CP-violating phase $\theta_{1'}$ ($0 \leq \theta_{1'}/\pi \leq 1$), and calculate the neutron EDM $|d_n|$. The results are shown in the fig.11. The results indicate that $|d_n|$ exhibits a significant dependence on $\theta_{1'}$: when $\theta_{1'}/\pi$ lies in the intermediate region (0.2-0.8), $|d_n|$ is relatively large, while it decreases significantly near the endpoints 0 or 1. For a fixed phase, $|d_n|$ decreases with increasing $m_{B'}$, indicating that a larger $m_{B'}$ leads to stronger suppression of the loop contribution. This behavior reveals the important role of the newly introduced B' boson mass and its associated CP-violating phase in the neutron EDM. Within the scanned parameter range, the calculated results can satisfy current experimental constraints.

Fig.12 shows the distribution of the neutron EDM d_n in the m_B (500GeV – 3000GeV) and

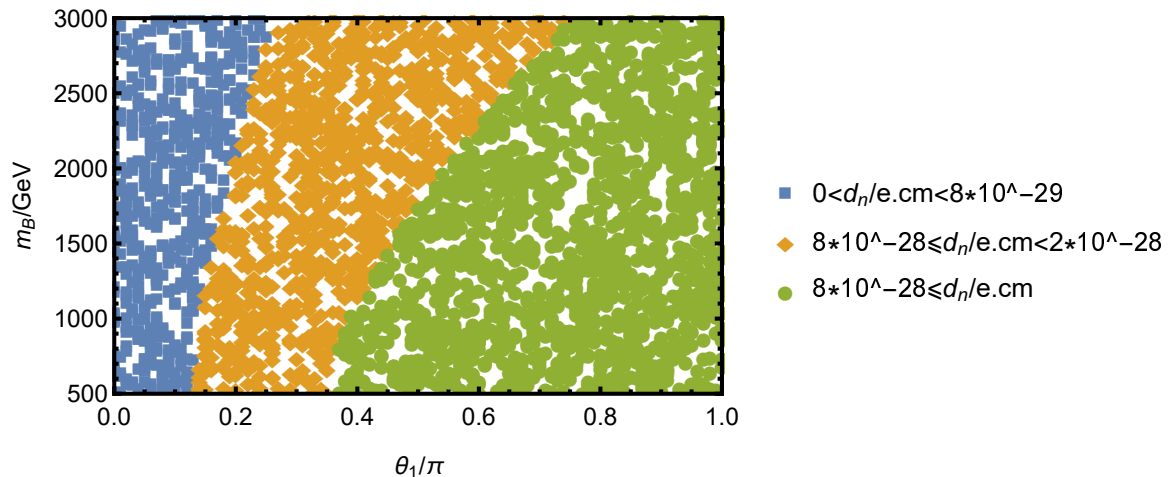


FIG. 12: The effects of m_B and θ_1 on d_n .

$\theta_1(0-\pi)$ parameter plane, with all other phases set to zero: $\theta_{1'} = \theta_2 = \theta_{\mu_H} = \theta_3 = \theta_{BB'} = 0$. The plot indicates that d_n exhibits a stepwise increase with rising θ_1 , demonstrating that θ_1 is a key parameter governing the magnitude of d_n . For a fixed θ_1 , d_n also increases as the vertical axis m_B rises from 500 GeV to 3000 GeV. These results in a clear synergistic enhancement between θ_1 and m_B : a larger θ_1 can yield a large EDM even with a smaller m_B . Specifically, d_n lies in the low-value region (blue) for $\theta_1/\pi \lesssim 0.2$, transitions to the intermediate-value region (orange) for $0.2 \lesssim \theta_1/\pi \lesssim 0.4$, and enters the high-value region (green) for $\theta_1/\pi \gtrsim 0.4$. The combined effect of these two parameters enables d_n to satisfy the relevant experimental constraints.

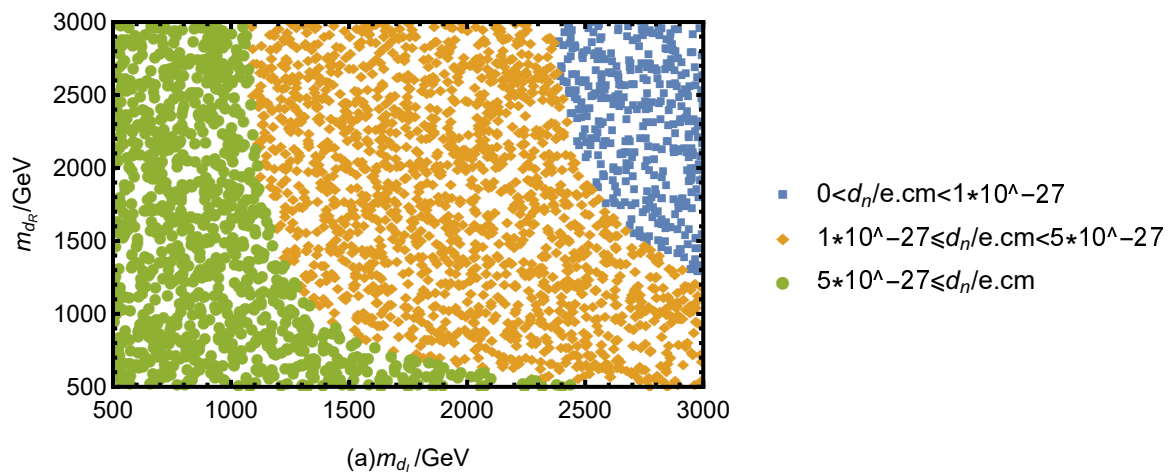


FIG. 13: The effects of m_{d_L} and m_{d_R} on d_n .

This fig.13 presents the graded distribution of the neutron EDM $|d_n|$ in the (m_{d_L}, m_{d_R})

(left-hand and right-hand down squark mass) parameter plane. The scanned parameter range is $500\text{GeV} - 3000\text{GeV}$. In this case, the phase $\theta_3 = \theta_2 = \theta_{\mu H} = \theta_{1'} = \theta_{BB'} = 0$, $\theta_1 = \frac{\pi}{3}$. The results show that d_n is significantly suppressed with increasing m_{d_L} and enhanced with increasing m_{d_R} , with the suppression effect of m_{d_L} being dominant. There is a clear competition and compensation relationship between the both: in the low m_{d_L} region, a high m_{d_R} can generate a high d_n (green region, $d_n \geq 5 \times 10^{-27}$ e.cm); when m_{d_L} is high, the enhancement effect of m_{d_R} is completely suppressed (blue region, $d_n < 1 \times 10^{-27}$ e.cm). The d_n in the green high-value region is close to the target sensitivity of future neutron EDM experiments, providing a clear parameter space constraint for model verification.

V. CONCLUSION

Within the framework of the N-B-LSSM, we systematically calculate the one-loop contributions to the EDMs of leptons and quarks via the MIA, and perform a comprehensive numerical analysis. This study clearly reveals the modulating effects of kinetic mixing parameters and novel CP-violating phases on EDMs. The results are summarized as follows:

In the lepton sector, the coupling parameter g_{YB} can modify the relative weights of different one-loop contribution terms and induce destructive interference regions. Phase parameters of the θ -type yield a typical behavior where EDMs oscillate periodically with a 2π cycle. In contrast, $\tan\beta$ enlarges the overall magnitude of EDMs primarily by enhancing the weights of chiral mixing, without changing the zero-point distribution structure of EDMs. Under the strict limitations of experiments, the electron EDM can be effectively suppressed through small phase values, high mass scales, or phase cancellation mechanisms. Notably, the phase cancellation mechanism allows for the existence of large CP-violating phases even when the particle mass is at the TeV scale, thereby improving the acceptability of the model.

The construction of the neutron EDM includes contributions from quark EDMs, quark CEDMs, and the Weinberg operator, resulting in richer parameter dependent features. $\tan\beta$ has a stable enhancing effect on the neutron EDM, whereas the newly introduced mass scale shows a suppressive trend. The strong phase θ_3 usually dominates the morphological characteristics of CP interference, while other phases such as $\theta_{1'}$ constitute secondary but independent sources of CP violation.

EDM experiments exert rigorous joint constraints on the kinetic mixing coupling pa-

rameters and novel CP-violating phases in the N-B-LSSM. In particular, high-precision measurements of the electron and neutron EDMs provide a clear observational window for testing this class of $U(1)_{B-L}$ extended supersymmetric models.

With a reasonable selection of parameters, the N-B-LSSM can simultaneously satisfy the current experimental upper limits on the EDMs of leptons and neutrons, and certain parameter spaces can even approach the detection sensitivity of future experiments. The MIA demonstrates good applicability in this model, enabling a clear elucidation of the regulatory mechanisms of CP-violating phases and various coupling parameters on EDMs. This work establishes a complete analytical framework and numerical benchmark for the systematic study of EDMs in B-L extended supersymmetric models, and provides solid theoretical support for the detection of CP-violating phases in new physics via high-precision EDM experiments in the future.

Acknowledgments

This work is supported by National Natural Science Foundation of China (NNSFC) (No.12075074), Natural Science Foundation of Hebei Province (A2023201040, A2022201022, A2022201017, A2023201041), Natural Science Foundation of Hebei Education Department (QN2022173), Post-graduate's Innovation Fund Project of Hebei University (HBU2024SS042), the Project of the China Scholarship Council (CSC) No. 202408130113. X. Dong acknowledges support from Fundação para a Ciência e a Tecnologia (FCT, Portugal) through the projects CFTP FCT Unit UIDB/00777/2020 and UIDP/00777/2020.

-
- [1] E. M. Purcell and N. F. Ramsey, Phys. Rev. **78** (1950), 807-807
- [2] M. Kobayashi and T. Maskawa, Prog. Theor. Phys. **49** (1973), 652-657
- [3] J. H. Christenson, J. W. Cronin, V. L. Fitch, et al., Phys. Rev. Lett. **13** (1964), 138
- [4] K. Abe et al. [Belle Collaboration], Phys. Rev. Lett. **87** (2001), 091802
- [5] B. Aubert et al. [BaBar Collaboration], Phys. Rev. Lett. **89** (2002), 201802
- [6] M. Pospelov and A. Ritz, Annals of Physics **318** (2005), 119-169
- [7] K. Inami, et al., [Belle], JHEP **04** (2022), 110
- [8] T. S. Roussy, L. Caldwell, T. Wright, et al., Science **381** (2023) no.6653, adg4084
- [9] C. Abel, S. Afach, N. J. Ayres, et al., Phys. Rev. Lett. **124** (2020) no.8, 081803
- [10] G. W. Bennett et al., [Muon (g-2)], Phys. Rev. D **80** (2009), 052008
- [11] S. Navas et al., [Particle Data Group], Phys. Rev. D **110** (2024) no.3, 030001
- [12] M. Dine, P. Huet, R. L. Singleton, et al., Phys. Lett. B **257** (1991), 351
- [13] A. G. Cohen and A. E. Nelson, Phys. Lett. B **297** (1992), 111
- [14] P. Huet and A. E. Nelson, Phys. Rev. D **53** (1996), 4578
- [15] J. M. Cline, M. Joyce and K. Kainulainen, JHEP **07** (2000), 018
- [16] D. E. Morrissey and M. J. Ramsey-Musolf, New J. Phys. **14** (2012), 125003
- [17] T. Falk and K. A. Olive, Phys. Lett. B **439** (1998), 71-80
- [18] T. Ibrahim and P. Nath, Phys. Rev. D **60** (1999), 099902
- [19] V. D. Barger, T. Falk, T. Han, et al., Phys. Rev. D **64** (2001), 056007
- [20] S. Di, S. M. Zhao, M. Y. Liu, et al., JHEP **08** (2025), 196
- [21] X. Y. Han, S. M. Zhao, L. Ruan, et al., Eur. Phys. J. C **85** (2025) no.2, 163
- [22] B. Holdom, Phys. Lett. B **166** (1986), 196-198
- [23] G. Bélanger, J. Da Silva and H. M. Tran, Phys. Rev. D **95** (2017) no.11, 115017
- [24] J. L. Yang, T. F. Feng, S. K. Cui, et al., JHEP **04** (2020), 013
- [25] U. Ellwanger, C. Hugonie, A.M. Teixeira, Phys. Rept. **496** (2010) 1-77.
- [26] V. Barger, P.F. Perez, S. Spinner, Phys. Rev. Lett. **102** (2009) 181802.
- [27] P.H. Chankowski, S. Pokorski, J. Wagner, Eur. Phys. J. C **47** (2006) 187.
- [28] J.L. Yang, T.F. Feng, S.M. Zhao, et al. Eur. Phys. J. C **78** (2018) 714.

- [29] T.F. Feng, L. Sun, X.Y. Yang, Nucl. Phys. B 800 221-252 (2008)
- [30] L.H. Su, S.M. Zhao, X.X. Dong, et al., Eur. Phys. J. C **81** (2021) 433.
- [31] S.M. Zhao, L.H. Su, and X.X. Dong, et al., J. High Energy Phys. **03** (2022) 101.
- [32] C.X. Liu, H.B. Zhang, J.L. Yang, et al., J. High Energy Phys. **04** (2020) 002.
- [33] E. Arganda, M.J. Herrero, R. Morales, et al., J. High Energy Phys. **03** (2016) 055.
- [34] J. Dai, H. Dykstra, R.G. Leigh, et al., Phys. Lett. B **237** (1990) 216; D.A. Dicus, Phys. Rev. D. **41** (1990) 999.
- [35] A. Manohar and H. Georgi, Nucl. Phys. B **234** (1984) 189-212.